J. Mech. Phys. Solids 212 (2026) 106564

Contents lists available at ScienceDirect

Journal of the Mechanics and Physics of Solids

journal homepage: www.elsevier.com/locate/jmps

Unveiling scaling laws for wrinkling in compressed fiber-reinforced bilayers at any elastic mismatch ⋆

Andrea Mirandola [a,b], Angelo R. Carotenuto [b,c], Arsenio Cutolo [b,c], Stefania Palumbo [b,c], Massimiliano Fraldi [b,c,d,*], Luca Deseri [a,*]

[a] *Department of Civil, Environmental and Mechanical Engineering, University of Trento, via Mesiano 77, 38123, Trento, Italy*
[b] *Department of Structures for Engineering and Architecture, University of Napoli "Federico II", Via Claudio 21 (buildings 6-7), 80125, Napoli, Italy*
[c] *Laboratory of Integrated Mechanics and Imaging for Testing and Simulation (LIMITS), University of Napoli Federico II, Italy*
[d] *Département de Physique, LPENS, École Normale Supérieure-PSL, Paris, France*

A R T I C L E I N F O

Keywords:
Scaling laws for wrinkling
Wrinkling of fiber-reinforced bilayers
Regime-transition in wrinkling
Symmetry-breaking in wrinkling
Wrinkling instabilities

A B S T R A C T

Wrinkling is a stress-induced bifurcation commonly observed in both natural and engineered systems, arising from physical or geometric mismatches in thin films, membranes, and various systems adhered to substrates with complex microstructures. In biology, such corrugations underly fundamental processes such as leaf morphogenesis, brain folding, vascular mechanics, swelling and drying, tissue growth or repair. While wrinkling in isotropic bilayers under imposed lateral compression is well characterized through established scaling laws–particularly for large film-to-substrate elastic mismatches–corresponding relations for fiber-reinforced bilayers remain comparatively widely underexplored.

In this work, we address this gap by analytically deriving asymptotic expansions for the onset of wrinkling when bifurcation occurs at both *small and finite strains* under prescribed compression, thereby *capturing the full spectrum of elastic mismatches* between the two sides of the bilayer. The film is modeled as an axially deformable elastic plate with bending stiffness, while the substrate is described using the Standard Reinforcing Model within finite elasticity.

Two distinct sets of scaling laws for the critical strain and wavenumber at the wrinkling onset are obtained, revealing *two regimes*: a *film-mediated* regime and a *substrate-governed* one. The *transition* between such behaviors is characterized by an *analytically derived threshold*, providing a clear criterion for selecting the appropriate scaling law for the case at hand.

Our framework applies to *biological systems*, as well as to *engineered bilayers*. For the latter, *symmetry-breaking* transition in the dispersion relation arises as the film-substrate mismatch decreases. Overall, this work provides a *unified theoretical framework* for rigorously obtaining *scaling laws for wrinkling in fiber-reinforced bilayers* across the *full range of elastic mismatches*, offering new insights into potentially analogous bifurcations in anisotropic compounds.

1. Introduction

Wrinkling is a well-known phenomenon that arises as a bifurcation mode for equilibrium in many biological and man-made systems. Various factors can cause corrugation, namely mechanical forces, such as compression, shear, pre-stress, thermal and osmotic

⋆ In memory of Miroslav Šilhavý (1949-2025).

* Corresponding authors.
E-mail addresses: fraldi@unina.it (M. Fraldi), luca.deseri@unitn.it (L. Deseri).

https://doi.org/10.1016/j.jmps.2026.106564
Received 2 October 2025; Received in revised form 10 January 2026; Accepted 15 February 2026
Available online 19 February 2026

effects, swelling, drying, shrinking, applied voltage, and growth (see, e.g., Cerda and Mahadevan, 2003; Chen and Yang, 2012; Liu et al., 2015; Pandurangi et al., 2022; Alawiye et al., 2019; Oguntade et al., 2024; Shen et al., 2024; Webber and Worster, 2024; Veldin et al., 2025; Wu et al., 2026).

Many systems exhibiting remarkable wrinkling involve bilayers (see, e.g., Genzer and Groenewold, 2006 among many others), typically formed by an extremely thin layer, a film, bonded to a very thick substrate. A key factor for such media is the stiffness mismatch between their perfectly adhering components, namely the film and the substrate, as they would deform in totally different ways if unconstrained. Of course, the perfect bonding between such mismatched components gives rise to compressive internal stresses that, once they reach a critical threshold, lead to wrinkling of the layer-substrate interface, hence of the film itself. Such corrugation manifests itself in periodic wavy patterns on the body's surface at hand, both at the onset of its occurrence and, very often, for further loadings.

Bilayers are frequently seen in fabricated devices (see, e.g., De Tommasi et al., 2010; Greaney et al., 2019; Ma et al., 2021; Khurana et al., 2022; Landis et al., 2022) and in nature (see, e.g., Hohlfeld and Mahadevan, 2011; Ciarletta et al., 2014; Balbi et al., 2015; Georges, 2017; Pocivavsek et al., 2019). Wrinkling of bilayers has influenced technological applications in recent years, such as electronics and sensor development (e.g., Koo et al., 2018; Wang et al., 2018; Qin et al., 2021; Li et al., 2022; Lee et al., 2022), as well as in surfaces designed to minimize frictional fluid drag (Lin et al., 2021), liquid crystal elastomers (Agrawal et al., 2012; Goriely and Mihai, 2021), structural colors (Tan et al., 2022; Zhou et al., 2020), origami (Mahadevan and Rica, 2005; Wong et al., 2016; Bae et al., 2017; Liu and James, 2024), and metamaterials (Silverberg et al., 2014; Zheng et al., 2017), among many others. Bilayers that form rugae have been extensively studied over the past few decades, with a primary focus on isotropic systems (see, e.g., Huang et al., 2005; Budday et al., 2017; Cao and Hutchinson, 2012; Akerson and Elliott, 2022; Ben Amar, 2025; Nagashima et al., 2025). For instance, in Liu et al. (2022), Cranston et al. (2011) it is shown how by knowing the critical strain and the corresponding wavenumber, it is possible to determine the elastic modulus of thin films undergoing wrinkling. Considerable attention has been given to the substrate and, over the years, authors have considered various constitutive models, along with "liquid" substrates (Pocivavsek et al., 2008; Brau et al., 2013) and, more recently, substrates with spatially-varying stiffness (O'Kiely et al., 2025). In the context of infinitesimal strains, Allen (1969) derived simple expressions for the critical strain and wavenumber for a fully isotropic bilayer, later expanded in Cao and Hutchinson (2012), Sun et al. (2011) to account for the initial prestretch of the substrate. On the other hand, when wrinkling occurs at moderate-to-finite strains, material nonlinearities of the substrate have been shown to play a key role in the response of the system even when bilayers are initially isotropic (e.g., see Hutchinson, 2013; Song et al., 2008; Cutolo et al., 2020).

Notable are the studies of the limiting cases. The first one is due to Biot (1963) who, in the context of isotropic finite elasticity and in the absence of any film, derived the critical stretch of a neo-Hookean half-space undergoing compression, proving that any wavelength is admissible for wrinkling in this case. In light of this result, a thin film bound to the substrate can certainly be interpreted as a "filter´´ for the resulting bilayer, allowing the system to wrinkle with a single wavenumber (Sharp et al., 2007). The other extreme scenario involves thin films subjected to compression resulting from applied extensional or tensile actions (see, e.g., Cerda and Mahadevan, 2003; Davidovitch et al., 2011; Vella et al., 2011; Chopin et al., 2015; Kudrolli and Chopin, 2018; Xin and Davidovitch, 2021; Wang et al., 2022; Healey, 2023; Venkata et al., 2023; Pamulaparthi Venkata et al., 2024; Venkata et al., 2025; Zhang and Kiendl, 2025), all in the absence of fibers. It is well known that, in this case, there is no indeterminacy of the wavenumber when wrinkling occurs. Here, a critical imposed elongation gives rise to wrinkling with a specific wavenumber (for a thorough analysis on this problem see, e.g., Puntel et al., 2011).

Within the context of linearized geometrical changes and strains, some papers addressed the attention towards both to isotropic viscoelastic bilayers (Mane and Huang, 2022) and to orthotropic substrates (Vonach and Rammerstorfer, 2000; Mirandola et al., 2023; Montanari et al., 2024). The former pushes its analysis to low elastic mismatches, although material and geometric nonlinearities are not accounted for in such analysis. Other papers analyzed wrinkling, folding, and creasing of fiber-reinforced biological bilayers (without a priori constraining the magnitude of the contractile strains), like in Stewart et al. (2016), for a specific model in the context of growth and prestress, and in Nguyen et al. (2020) for preliminary experimental, analytical, and computational analysis induced by lateral compression.

From a design standpoint, it is certainly quite useful to have *scaling laws* at our disposal for the phenomenon at hand. Those should show how the critical strain and wavenumber scale with the main physical quantities characterizing the system. Unfortunately, it is only for a few cases that scaling laws for the wrinkling onset have been found over the decades. This work aims at overcoming such a drawback, especially given the importance and the potential of biological (see, e.g., Pitre, 2024; Youn et al., 2024 and referenced cited therein) and manufactured bilayers (see, e.g., Zheng et al., 2017; Ramachandran et al., 2021). On the one hand, the asymptotic expression provided by Cao and Hutchinson (2012) for pre-stretched fully neo-Hookean bilayers is most certainly a key milestone. Analog outcomes can be found in Cai and Fu (1999) and in Sun et al. (2011), although the latter delivers implicit laws for the very same case of fully isotropic bodies. All of the above relate to the result due to Allen (1969) obtained when wrinkling occurs for strains whose magnitude is $\leq 10^{-3}$, i.e. within the "infinitesimal" strains regime, occurring when the film-to-matrix mismatch is very high (namely $\geq 10^{-4}$). Specifically, there the analysis holds for linear anisotropic substrates bonded to thin linear elastic films. Material nonlinearity for some special cases of anisotropic layer (i.e., liquid crystal elastomers) bonded onto an isotropic hyperelastic substrate has also been recently examined in the literature, accounting for non-infinitesimal strains (e.g., see Goriely and Mihai, 2021).

Besides a few recent contributions (see, e.g., Nguyen et al., 2020, for preliminary analysis and Liu, 2024; Liu et al., 2025b), situations in which moderate wrinkling strains occur in bilayers formed by isotropic elastic films bonded to a nonlinear anisotropic substrate are much less studied. The latter work, focuses on a new, rigorous, and thorough analytic study of local post-wrinkling of fiber-reinforced bilayers, which goes beyond the focus of this present work (although it is partially covered here in Supplementary material G, through a computational analysis of the ruga's amplitude, detecting further bifurcations leading to period doubling and

List of Symbols

Auxiliary symbols

Δ	Difference between the lateral Biot's stretch $\Delta = \lambda_1 - \lambda_B$
Λ_k	Modulation function of the asymptotic strain and wavenumber
$\mathcal{M}_{ij}^{(m)}$	The ij-th component of the matrix $\mathbf{M}$ is given by $\sum_{m=0} \mathcal{M}_{ij}^{(m)} k_h^m$
$\mathcal{N}_{\eta\omega}$, $\mathcal{D}_{\eta\omega}$	Coefficients defining the critical strain and non-dimensional wavenumber
ω_1, ω_2	Coefficients appearing in the multiplicative decomposition $\mathcal{N}_{02} = \omega_1\omega_2$
ω_{10}, ω_{11}	Approximation of ω_1
$\mathbf{M}$	Coefficient matrix of the interface equilibrium
ξ_i	Auxiliary coefficients defining the parameter α
ζ_i	i-th term of the modulation function Λ
c_i	i-th coefficient of the dual scaling law of the critical strain and wavenumber
I_{4m}	Fourth invariant of $\mathbf{C}$ referred to the m-th fiber family ($\mathbf{t}_m \cdot \mathbf{C}\mathbf{t}_m$)

Constitutive parameters

γ	Volumetric concentration mediated stiffness of the fibers
κ	Orientational dispersion of the fibers ($0 \le \kappa \le 1/3$)
μ_M, μ_L	Half of the shear modulus of the matrix (μ_M) and of the layer (μ_L), respectively
ν_L	Poisson's ratio of the film (also called "layer" through the manuscript)
$\rho_{ML} = \mu_L/\mu_M$	Mismatch ratio between the matrix and the film
$\rho_{LM} = \mu_L/\mu_M$	Mismatch ratio between the film and the matrix
$\rho_{FM} = \gamma/\rho_{ML}$	Mismatch ratio between the fibers and the matrix
$\mathbf{H}_m$	Structure tensor of the m-th fiber family
$\mathbf{t}$	Unit vector of the mean angle of a fiber family
θ	Angle of a fiber family with respect to the horizontal axis
E_L	Young's modulus of the film
h	Thickness of the film

Kinematics

$\mathcal{A}$	Amplitude of the wrinkles
$\varepsilon_{cr}, k_{h,cr}$	Critical strain and non-dimensional wavenumber
$\lambda_h = k_h^{-1}$	Inverse of the non-dimensional wavenumber
λ_i	Stretch along the i-th direction
$\mathbf{C}$	Right Cauchy tensor
$\mathbf{C}_0, \mathbf{F}_0$	Right Cauchy and deformation tensors evaluated during the homogeneous deformation
$\mathbf{C}_{01}$, $\mathbf{F}_1$	First-order perturbation of right Cauchy and deformation tensors due to wrinkling
$\mathbf{F}$	Deformation gradient
ε^L	Longitudinal strain
$\varepsilon_{cr,nh}, k_{h,cr,nh}$	Critical strain and non-dimensional wavenumber of a neo-Hookean bilayer
λ_B, ε_B	Critical stretch and strain of Biot's bifurcation problem of a neo-Hookean half-space
k, λ	Wavenumber and wavelength of the wrinkle ($\lambda = 2\pi/k$)
$k_h = kh$	Non-dimensional wavenumber
u_i	Displacement along the i-th direction
X_i	i-th direction of the reference system (1:horizontal, 2: vertical)
x_i	i-th direction of the current system

Other symbols

$(\bullet)_{,j}$	Partial derivative with respect the j-th direction X_j
α	Coefficients defining the spatial damping of the wave along the depth of the substrate
δ	Perturbation parameter
$\mathbf{e}_i$	Unit vector of the i-th direction
$\mathbf{I}$	Identity tensor
$\tilde{\bullet}$	Linear combination of the eigenfunctions $\bullet$
C_i	Weights of the linear combination $\tilde{\bullet}$

Stress and energy

$\mathbf{P}$	First Piola-Kirchhoff stress tensor
E_0	E_m evaluated during the homogeneous deformation
E_m	$\gamma E_m^2/2$ defines the m-th fiber family contribution to the energy
E_{m1}	First-order perturbation of E_m due to wrinkling

p_0	Internal pressure to ensure incompressibility during the homogeneous deformation
p_1	Internal pressure to ensure incompressibility due to wrinkling
W	Strain energy density

quadrupling, then folding). There, a very non-trivial extension of Koiter's approach (undertaken in Hutchinson, 2013; Akerson and Elliott, 2022 for neo-Hookean systems), has been worked out.

Nevertheless, scaling laws governing the bifurcation phenomena in question remain unaddressed, including those pertaining to the onset of wrinkling. With this as a primary focus, self-consistent parametric and explicit asymptotic expressions have been recently provided in Mirandola et al. (2023) for the case of infinitesimal strains. There, bilayers formed by soft fiber-reinforced substrates and orders of magnitude stiffer films undergoing an imposed lateral contraction have been considered. In particular, an explicit modulation function depending on the fiber's orientation and dispersion has been found to amplify the scaling laws provided in Allen (1969), Cao and Hutchinson (2012) for the case of no prestretch and highly mismatched isotropic bilayers. The explicit scaling laws obtained in Mirandola et al. (2023) are shown to well approximate the key wrinkling features, i.e. the critical strain and wavenumber, obtained analytically for highly mismatched fiber-reinforced bilayers. It is worth noting that, as functions of the fiber angle, these quantities exhibit *symmetric behavior* about 45°. In biological materials, this is unlikely to occur, as fibers are recruited to participate in their response as long as they are elongated (see, e.g., Holzapfel et al., 2000; Robertson and Watton, 2013; Holzapfel and Ogden, 2017; Lu et al., 2025). On the contrary, this can happen in man-made composites whenever fibers are sufficiently transversely confined by the loaded matrix, so that they can bear compressive stresses away from experiencing (micro)buckling or other collapse mechanisms (see, e.g., Kurashige, 1983; Budiansky and Fleck, 1993; Slaughter et al., 1996; Fleck, 1997; Niu and Talreja, 2000; Opelt et al., 2018; Thomson et al., 2019). In this way the fiber reinforcement is effective both under contraction and elongation of the fiber's themselves, thereby inducing a bilateral response to compressive and tensile loads to the resulting composite. Consequently, the corresponding scaling laws display the symmetry highlighted above, although for very small wrinkling strains it is expected that only when fibers are sufficiently inclined with respect to the loading direction that they can experience elongation.

Even when the bilateral behavior discussed above is effective, there is an indication that the onset of symmetry loss is detectable for matrix-to-film elastic mismatches of the order of 10^{-3}, for which a slight deviation from the symmetric behavior highlighted above is noticeable (see, e.g., Nguyen et al., 2020; Mirandola et al., 2023). Moving towards lower values than 10^{-3} highlighted above, the *symmetry breaking* for the wrinkling features as functions of the fiber angle is recorded. In this respect, *there is a substantial lack of knowledge regarding the scaling laws for compressed fiber-reinforced bilayers with moderate-to-low layer vs matrix elastic mismatches*. Of course, the lower such a mismatch gets, the higher the strain required for wrinkling to appear. The magnitude of such critical strain can become quite significant, as it can get asymptotically close to the Biot's limit of the fiber-reinforced substrate at hand. This can occur when the mediating role of the thin layer versus the substrate on the wrinkling onset tends to weaken (for instance, as shown in Section 4, this can happen at values of the matrix-film elastic mismatch order of less than 1-to-5).

In summary, *here, and for the first time in the literature, scaling laws for the critical strain and corresponding wavenumber are rigorously derived for the onset of wrinkling in fiber-reinforced bilayers with no restrictions on the substrate-film stiffness mismatch*. This largely extends the work by Mirandola et al. (2023) in a very non-trivial way to corrugation instabilities at moderate to finite strains.

This present work is organized as follows.

In Section 2, we describe the analytical model of the bilayer. Due to its thinness relative to the assumed (infinite) depth of the substrate, the film is modeled as a deformable plate, undergoing bending and contraction, perfectly bonded to an infinitely deep hyperelastic substrate (see, e.g., Shield et al., 1994, Sun et al., 2011). With the aim of expanding this analysis to soft and low mismatched fiber-reinforced composites, while retaining the capability of covering stiffer and more highly mismatched system within the same procedure, it is for the sole sake of illustration that the constitutive equation chosen here for the substrate is based on the *Standard Reinforcing Model*, hereafter referred to as *SRM* (Qiu and Pence, 1997; Guo et al., 2007; Chagnon et al., 2015; Kurashige, 1981; Triantafyllidis and Abeyaratne, 1983). It is worth noting that this accounts for fiber's orientational dispersion in the most simplistic way (Shashwati, 2022; Melnik et al., 2015) and it can be obtained as a limiting case of the law proposed by Holzapfel et al. (2000), Gasser et al. (2005). The latter and its variants (see, e.g., Federico and Gasser, 2010; Federico et al., 2011; Pandolfi and Vasta, 2012; Gizzi et al., 2018, 2024 among many others) are well suited for fiber-reinforced biological tissues. Nevertheless, their details are known not to significantly influence the wrinkling onset (see Liu et al., 2025b), thereby indicating that the SRM law may suffice for this aim. The analytical solution of the interface balance is then provided in this section for the three-dimensional (3D) substrate (under plane-strain conditions) obeying the SRM law. Besides the symmetry breaking discussed above, a comparative analysis of the dispersion properties for two suitable models for fiber-reinforced bilayers is performed in Section 2. In the first one, the film is modeled as an extensible plate supporting bending. For the second model at hand, such a film is regarded as a fully 3D body undergoing plane strain. Regarding the onset of wrinkling, the analysis performed in this section shows that modeling the thin film like in Shield et al. (1994) rather than a fully 3D medium gives quite accurate estimates of the wrinkling features at its onset. The analytic results provided in Section 2 (details on the calculations are reported in Supplementary material A) set the stage for providing consistent expansions of the expressions for the critical strain and wavenumber at the onset of wrinkling, no matter what the matrix-to-layer mismatch and whatever orientation and concentration-mediated fiber-matrix stiffness ratio.

As observed before, the occurrence of wrinkling in medium-to-low elastic mismatched bilayers arises at moderate-to-large strains before wrinkling. In Section 3, a rigorous asymptotic analysis is performed for fiber-reinforced bilayers with matrix-layer mismatches up to that range, for which the film mediates the onset of the corrugation. Finding scaling laws in such a non-linear setting required expanding in Section 2 the formulation proposed in Mirandola et al. (2023), which is effectively suitable for small strains. Of course, the necessary asymptotics yielding the results is way more challenging than in the previous case. To do so, the conceived procedure relies upon Puiseux series (see, e.g., Poteaux and Rybowicz, 2012), namely a generalization of Taylor expansions allowing for fractional powers (see Supplementary material C for the methodology and Supplementary material B for auxiliary calculations). The main advantage of this approach is that *both the exponents and the coefficients of the series must be systematically calculated*; thus, unlike other approaches (e.g., the perturbation method, adopted in Mirandola et al., 2023), it requires no extra assumptions on the exponents of each single term of the expansion. Furthermore, all such terms are parametric expressions of the key features characterizing the fiber-reinforced bilayers, such as the matrix-to-layer elastic mismatch, the concentration-mediated fiber-matrix mismatch (and concentration) relative to the matrix, the fiber's orientation, and their orientational dispersion. Due to the involved form of the obtained terms, the Puiseux series procedure's bare-bones outcomes may not be so practical for the reader to utilize the obtained scaling laws. To this end, more compact, useful, and revealing asymptotic expressions are sought by simultaneously exploring (a) a dilute concentration mediated fiber-to-matrix elastic mismatch approximation and (b) small to moderate strains. For this reason, further Taylor expansions of both Puiseux expressions of the wavenumber and the critical strain accounting for (a) and (b) are performed. Unlike the infinitesimal-strains case, the new scaling laws, namely (19), (20) (supported by (21), (22a), (22b), (22c)), are implicit and cover the whole spectrum of film-mediated wrinkling, namely from highly-to-medium-low mismatched fiber-reinforced bilayers, hence from very small-to-moderate wrinkling strains. Noticeably, by letting the concentration-mediated fibers-to-matrix parameter to zero, i.e., for fiber-less (hence isotropic) compressed and moderate-to-fairly low mismatched bilayers, the obtained scaling law for the wrinkling strain at its onset is consistent with the one obtained in Hutchinson (2013). An explicit scaling law for the critical strain has also been derived, although it applies over a more limited range than (20).

Although the analysis discussed above applies to bilayers in which the film primarily governs the onset of wrinkling, the presence of reinforcing fibers in the substrate matrix is expected to induce a transition from this film-dominated regime to a substrate-mediated one. Depending on the degree of reinforcement, such a transition may occur for relatively moderate matrix-to-film elastic mismatches. In contrast, for fiberless (and therefore isotropic) bilayers, it is known to take place when the matrix and film moduli are comparable. This circumstance has been extensively investigated under the assumption that both the film and the substrate are fully three-dimensional isotropic bodies subjected to plane-strain compression (see, e.g., Wang and Zhao, 2013; Fu and Ciarletta, 2015; Zhao et al., 2015; Auguste et al., 2017). In such cases, several competing bifurcation modes have been identified by looking at post-wrinkling analysis, which is out of the scope of this paper (as mentioned above, for fiber-reinforced bilayers this has been studied by Liu, 2024; Liu et al., 2025b). For fully isotropic bilayers, available studies near bifurcation document wrinkles that: (i) transition directly to creases, (ii) undergo period doubling before creasing, or (iii) undergo successive period doubling and quadrupling before folding. The presence of reinforcing fibers within the substrate does, of course, yield a stiffer effective behavior of the bilayer, thereby exhibiting different post-bifurcation modes relative to the isotropic case discussed above (in Supplementary material G a brief discussion about the corrugation amplitude and associated post-wrinkling modes in relevant cases is reported). Studies addressing wrinkling in bilayers with similar elastic mismatch conditions, in which *the film is viewed as an extensible thin plate with bending rigidity*, remain scarce in the literature, even in the case of fully isotropic systems (see, e.g.,Supplementary material E for a detailed analysis of such a model).

Of course, relative to the isotropic bilayers highlighted above, the presence of reinforcing fibers in the substrate is expected to make major differences in the bifurcation behavior even when the mismatch between the matrix and the film is reduced. In particular, the interplay between the substrate and the layer in terms of mediating the onset of wrinkling not only depends on the matrix-to-layer mismatch, but also on the degree of fiber reinforcement (i.e., on their orientation, stiffness, concentration). It follows that the asymptotics provided in Section 3 are not capable to capture the wrinkling features of bilayers for which the substrate starts competing with the film as mediator of the wrinkling onset. Indeed, such systems are characterized by significant wrinkling strains at their onset, which can get close to their corresponding Biot's value in the limit of vanishing films. The required analysis is performed here in Section 4. Depending on the effectiveness of the fiber reinforcement, the value of the layer-vs-matrix mismatch at which the substrate starts overtaking the role of the film upon mediating the wrinkling onset of the bilayer spans a very wide range, starting at fairly moderate values. In the complete absence of fibers, such a value is achieved by approaching 1 from below. For a fully three-dimensional model, 1 is exactly when the Biot's limit $\varepsilon_B \approx 0.4563$ is attained. Reinforcing fibers tend to shift backward (relative to 1) the mismatch value at which the transition from film-mediated to substrate-dominated wrinkling occurs. This effect can, in fact, be very significant, as it is discussed in Section 4. What has been just described represents essentially a "material phase transition", governed by a threshold of the matrix-vs-layer elastic mismatch at which the switching of regime occurs. This can be recognized by the fact that a specific "amount of reinforcement" exists for which a slightly lower value than this critical threshold allows the compressed bilayer to behave anisotropically and with a film-mediated wrinkling behavior. On the other hand, bilayers with a slightly higher value of critical reinforcement become substrate-dominated through an isotropization of their behavior. The encountered threshold for such a transition is analytically determined by (28) in this section. Furthermore, we also present a phase diagram using the same threshold for two distinct scenarios in Fig. 8: one in which fibers reinforce the composite only when elongated, and another in which they enhance the substrate´s response when shortened (it is only for this latter case for which the threshold above could also be pushed forward to values higher than 1, and this is briefly discussed in this same section). Furthermore, among other features, dispersion properties of the whole bilayer displayed in Fig. 9, provided for the exact solutions of the fully 3D problem (in plane-strain conditions, not explicitly reported in the paper), do confirm the transition discussed above.

The regime's transition, as expected, has a significant impact on the scaling of the onset of wrinkling. Indeed, the asymptotics obtained in Section 3 fail to work. This is primarily because, asymptotically, as the bifurcation regime becomes less and less mediated by the film, its Young modulus tends to vanish relative to that of the substrate's matrix. At the same time, upon utilizing the plate model of Section 2, the wavenumber significantly drops to much lower values in this case, thereby increasing the wavelength of the bifurcation mode after the transition. It is by factoring the exact solutions for the wrinkling onset provided in Section 2 in a dual way than before that the Puiseux asymptotics delivers the first information about the appropriate scaling covering the regime transition. Exactly as it happened for the direct asymptotics worked out in the previous section, the obtained expressions are not yet useful for interpreting the phenomenon during this regime's transition. In analogy with what has been done in Section 3, it is through a further Taylor expansion of both the Puiseux expressions for the wrinkling features that useful information about the scaling is revealed. Here, such further expansions are worked out by expanding for the case of (a) the small concentration mediated fiber-to-matrix mismatch, and (b) for the imposed contractile strain near the Biot's limit (for the fiber-less, hence isotropic, case). It is in this context that binomial, and implicit (like in the direct regime) scaling laws, (38) and (40), for both the critical wavenumber and the strain are first found. The latter is actually shown to always represent an asymptotic upper bound for the critical strain at the very onset of wrinkling. Further investigations near the 3D fiber-less transition lead to two explicit forms for the critical strain's scaling, i.e., relations (44) and (45) (primarily depending on the matrix-to-layer mismatch), which show a better average approximation of the exact wrinkling. Among other things, this section further addresses how the regime's threshold interlaces with the two sets of scaling laws found here and in Section 3 by varying the degree of reinforcement. Furthermore, all the other asymptotic expressions found for both the critical strain and the corresponding wavelength are compared for paradigmatic cases. Conclusions are then drawn in Section 5.

Furthermore, within the Supplementary Material, containing nine sections, besides the ones cited above, the others cover a variety of explicit calculations and auxiliary considerations useful for the obtained scaling laws.In particular, Supplementary material D gives the details of the "diluted approximation´´ of such laws in the direct regime, utilized to make predictions on both features of the wrinkling onset for high-to medium-low layer-to-matrix mismatches. The new scaling laws particularized to the case of neo-Hookean bilayers at any mismatch are covered in Supplementary material E, while the case of one family of fibers is analyzed in Supplementary material F. As mentioned above, Supplementary material G briefly analyzes both the scaling of the wrinkling right after its onset and subsequent post-bifurcations, while Supplementary material H displays the relative errors of the obtained asymptotics and scaling laws against the exact solution of the plate model for each selected case. Finally, Supplementary material I reports the comparison between the non-analytically obtained, ad-hoc scaling law for the wrinkling strain and the corresponding asymptotic laws derived in the present paper, starting from the Puiseux expansions introduced above.

2. Analytical model: small-to-finite strains

As stated in the introduction, while more complex and realistic constitutive laws could be applied to biological and man-made fiber-reinforced materials, for simplicity and illustration, the mechanical response of the substrate here is described by using the SRM law mentioned above. This characterizes the behavior of an anisotropic material by additively splitting the strain energy density into two quadratic contributions. The first one, $W_{s,\text{matrix}}$, represents the strain energy density of the neo-Hookean matrix, i.e.

$$W_{s,\text{matrix}} = \mu_M (I_1 - 3) \quad \text{with } I_1 := \text{tr}(\mathbf{C}), \tag{1}$$

where $\mathbf{C} = \mathbf{F}^T\mathbf{F}$ is the right Cauchy tensor, $\mathbf{F}$ is the deformation gradient and μ_M is half the shear modulus of the matrix. The second term in the additive decomposition, denoted here by $W_{s,\text{fibers}}$, is provided by the presence of fibers, and it is given by the following expression:

$$W_{s,\text{fibers}} = \frac{\gamma}{2} \sum_{m=1}^{N} E_m^2, \tag{2}$$

with N the number of family fibers embedded into the matrix and γ representing a fiber's concentration-mediated elastic modulus. The quantity E_m is a function of the fourth pseudo-invariant I_{4m} defined as follows:

$$E_m = \kappa(I_1 - 3) + (1 - 3\kappa)(I_{4m} - 1) \quad \text{and} \quad I_{4m} = \mathbf{t}_m \bullet \mathbf{C}\mathbf{t}_m, \tag{3}$$

where $\mathbf{t}_m = (\cos\theta, \sin\theta, 0)$ is the unit vector representing the mean angle of a family of fibers. In the sequel, we consider two families of fibers ($N = 2$) oriented at an angle $\pm\theta$ relative to the horizontal axis X_1 (refer to Fig. 1). The fiber dispersion κ can assume values between 0 (perfect alignment of the fibers along a given direction θ) and $1/3$ (random distribution of the fibers). Note the coupling between the isotropic and anisotropic parts in the definition of E_m in (3), as E_m depends on the first, angle-independent invariant. A complete decoupling only occurs when there is a perfect fiber polarization along an angle $\pm\theta$, i.e. when $\kappa = 0$. Moreover, it is worth noting that E_m represents a Green-Lagrange strain-like measure, describing the strain in the direction of the fiber family oriented along $\mathbf{t}_m$ (Gasser et al., 2005). Finally, the corresponding strain energy density of the fiber-reinforced substrate takes the following form:

$$W_{s,\text{SRM}} = W_{s,\text{matrix}} + W_{s,\text{fibers}}. \tag{4}$$

Obviously, the presence of $W_{s,\text{fibers}}$ in the energy density makes the substrate's response anisotropic.

To analyze the onset of wrinkling, a perturbation of the motion and pressure fields has been superimposed on those caused by a homogeneous, in-plane (potentially large) contraction induced through a compression along the direction X_1. Then, the bifurcation condition has been obtained by using a small-on-large approach, widely employed in literature to analyze bilayer bifurcation

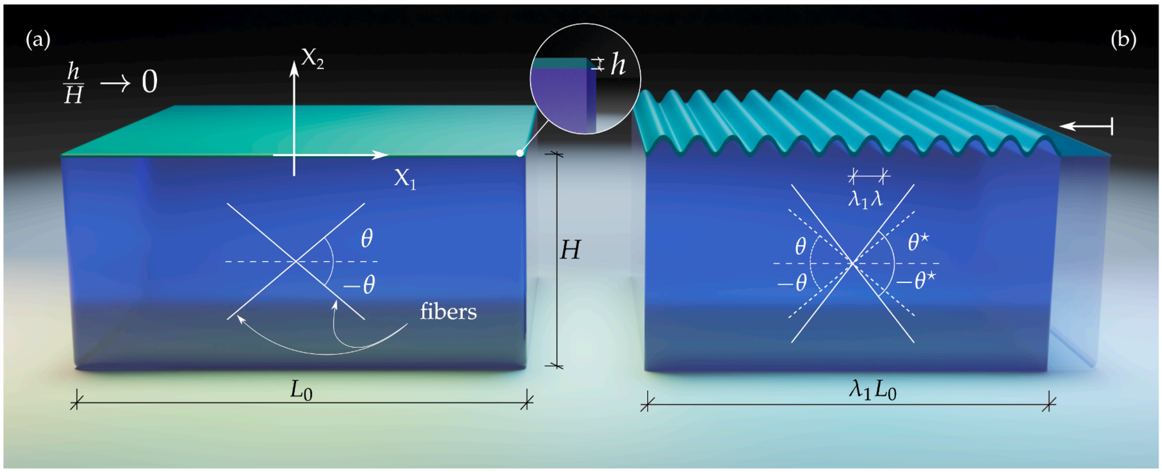

Fig. 1. Schematic of the plane strain bilayer model. Two fiber families are embedded within a neo-Hookean matrix, oriented at angles $\pm\theta$ relative to the reference axis X_1 (a). The substrate has a depth significantly greater than the layer thickness ($h/H \to 0$) and a rest length L_0. Under a contractile strain λ_1 (associated with the deformation ε^L), the bilayer uniformly deforms until wrinkling occurs (b), at a critical stretch $\lambda_{1,cr} = 1 - \varepsilon_{cr}$. During the homogeneous compression, the relative angle $\theta^\star$ changes, according to the relation $\theta^\star = 1/2 \arccos\left(\left(\mathbf{Ft}_1 \bullet \mathbf{Ft}_2\right)/\left(|\mathbf{Ft}_1||\mathbf{Ft}_2|\right)\right)$.

phenomena (see, e.g., Cao and Hutchinson, 2012, Hutchinson, 2013, Wang et al., 2023 and references cited therein). Following the approaches of Nguyen et al. (2020) and Sun et al. (2011), a perturbed in-plane lateral contraction $\mathbf{x} := (x_1, x_2)$ for the substrate is considered as follows:

$$x_1 = \lambda_1 X_1 - \delta\alpha\lambda_1^2\lambda \sin(kX_1)\mathrm{e}^{\alpha k X_2} + \mathcal{O}\left(\delta^2\right), \tag{5a}$$

$$x_2 = \lambda_2 X_2 + \delta\lambda \cos(kX_1)\mathrm{e}^{\alpha k X_2} + \mathcal{O}\left(\delta^2\right), \tag{5b}$$

$$p = p_0 + \delta p_1 \cos(kX_1)\mathrm{e}^{\alpha k X_2} + \mathcal{O}\left(\delta^2\right), \tag{5c}$$

where $0 < \lambda_1 \le 1$, and p is the above-mentioned hydrostatic pressure that maintains the isochoricity constraint.

Upon imposing isochoricity and plane strain condition of the homogeneous deformation prior to the superimposed perturbation, the stretch along direction X_2 is $\lambda_2 = \lambda_1^{-1}$. The constants p_0, p_1, and α will be determined by imposing the appropriate boundary conditions. Eqs. (5a) and (5b) indicate that, as wrinkling deforms the surface with a sinusoidal pattern, characterized by a wavelength λ. For further developments, it is convenient to relate this to a dimensionless wavenumber, k_h, defined as follows:

$$k_h := kh = 2\pi h/\lambda, \tag{6}$$

as the standard wavenumber, k, is instead set by the relation $k = 2\pi/\lambda$. Finally, the superimposed field due to wrinkling has been introduced by a perturbation whose amplitude is scaled through the constant $\delta \ll 1$. Details on the balance of linear momentum for the substrate are reported in Supplementary material A. For this, a key parameter is the fiber's concentration-mediated fibers-matrix elastic mismatch, defined as follows:

$$\rho_{FM} := \gamma/\mu_M. \tag{7}$$

As noted earlier in this section, the thickness of the layer is very small compared to the substrate's height and the wrinkling wavelength. Hence, the upper layer can be reasonably modeled as an extensible linear elastic plate exhibiting bending rigidity (Shield et al., 1994). Therefore, the balance of linear momentum at the interface between the film and the substrate can be cast in the following form (Shield et al., 1994):

$$\frac{E_L h}{1-\nu_L^2}\left(\frac{h^2}{3}\widetilde{u}_{2,1111} - \frac{h}{2}\widetilde{u}_{1,111} + \varepsilon^L \widetilde{u}_{2,11}\right) + \widetilde{P}_{s22}(x_1, 0) = 0, \tag{8a}$$

$$\frac{E_L h}{1-\nu_L^2}\left(\widetilde{u}_{1,11} - \frac{h}{2}\widetilde{u}_{2,111}\right) - \widetilde{P}_{s12}(x_1, 0) = 0, \tag{8b}$$

where

$$\varepsilon^L := 1 - \lambda_1 \tag{9}$$

is the defined by this relationship as the magnitude of the contractile *nominal* longitudinal strain that matches the absolute value of the longitudinal component of the gradient of the finite displacement $U_i := (\lambda_i - 1)X_i$, $i = 1, 2$, (which can also be evaluated from (5a) and (5b) after setting $\delta = 0$). Here, $\widetilde{u}_i = \widetilde{x}_i - \lambda_i X_i$, $(i, j = 1, 2)$ represents the i-th component of the incremental displacement corresponding to (A.15) in supplementary. Furthermore, $\widetilde{P}_{si2}(x_1, 0)$, $i = 1, 2$ are the traction components (see (A.15c) in supplementary for their expressions) arising from the substrate at the considered interface. Here, the Young modulus and Poisson ratio of the layer are denoted by E_L and ν_L, respectively.

As shown by Nguyen et al. (2020), Mirandola et al. (2023), and by many others, a key parameter for the analysis of the mechanics of the bilayer is the stiffness mismatch between the matrix and the layer, ρ_{ML}, defined as follows:

$$\rho_{ML} := 6\mu_M/E_L. \tag{10}$$

In this work, the order of the subscript letters indicates the position within the ratio: for instance, ρ_{FM} defined in (7) is equal to the stiffness of the fibers γ (F) over that of the matrix μ_M (M). As discussed in detail in Supplementary material A , the balance equations, (8a) and (8b), and the ansatz for the deformation, (5a), (5b), specified by using (A.15a)–(A.15c) in supplementary, lead to the system (A.16) in supplementary. Its singular equation, Eq. (A.18) in supplementary, can then be solved for the corresponding strain. This yields the following expression for the critical value for the lateral strain introduced in (9):

$$\varepsilon^L = \frac{\mathcal{N}_{02}\rho_{ML}^2 + \mathcal{N}_{11}k_h\rho_{ML} + \mathcal{N}_{21}k_h^2\rho_{ML} + \mathcal{N}_{31}k_h^3\rho_{ML} + \mathcal{N}_{40}k_h^4}{\mathcal{D}_{11}k_h\rho_{ML} + \mathcal{D}_{20}k_h^2}, \tag{11}$$

where the coefficients $\mathcal{N}_{\alpha\beta}$ and $\mathcal{D}_{\alpha\beta}$ are defined by (A.19) in supplementary. Upon following the procedure by Pence and Song (1991), Yue et al. (1994), and applied later by Sun et al. (2011), the *optimality* condition is imposed to Eq. (A.18) in supplementary, i.e., $\partial\varepsilon^L/\partial k_h = 0$. Differentiation of the (11) with respect to k_h yields

$$\begin{aligned} &2k_h^5\mathcal{D}_{20}\mathcal{N}_{40} + k_h^4\rho_{ML}\left(\mathcal{D}_{20}\mathcal{N}_{31} + 3\mathcal{D}_{11}\mathcal{N}_{40}\right) + 2k_h^3\rho_{ML}^2\mathcal{D}_{11}\mathcal{N}_{31} + \\ &\qquad + k_h^2\rho_{ML}\left(\rho_{ML}\mathcal{D}_{11}\mathcal{N}_{21} - \mathcal{D}_{20}\mathcal{N}_{11}\right) - 2k_h\rho_{ML}^2\mathcal{D}_{20}\mathcal{N}_{02} - \rho_{ML}^3\mathcal{D}_{11}\mathcal{N}_{02} = 0. \end{aligned} \tag{12}$$

Therefore, Eqs. (11) and (12) lead to a highly nonlinear system whose solution in terms of the pair (ε^L, k_h) yields the critical nominal strain ε_{cr} and the dimensionless critical wavenumber $k_{h,cr}$ at the onset of wrinkling. As pointed out by Holzapfel et al. (2000), biological fibers (i.e., collagen) do not store energy if shortened. This implies that $I_{40} \geq 1$, where I_{40} is defined by (B.5) in supplementary, leading to the following admissibility conditions (represented in the phase diagram Fig. 8 together with other information discussed in Section 4):

$$\begin{aligned} 1 - \tan\theta \leq \varepsilon^L < 1, &\qquad \text{if } 0 \leq \theta \leq \pi/4 \\ 0 \leq \varepsilon^L < 1, &\qquad \text{if } \pi/4 \leq \theta < \pi/2. \end{aligned} \tag{13}$$

This has first been obtained by Liu et al. (2025b) by using the contractile stretch λ_1, while here it has been recast in terms of the magnitude of its corresponding nominal strain, ε^L. Throughout this paper, the gray color is used to represent the zone ruled out by the inequality (13).

However, the solution obtained by considering active compressed fibers, i.e., contributing to stiffen the materials at hand, is always reported in the analysis of this paper as long as the compression borne by the contracted, and transversely-confined, fibers does not exceed their buckling stress (see, e.g., Sharma et al., 2023, Hamzat et al., 2025 among many others), and no other compression-triggered failure modes get activated (see, e.g., Budiansky and Fleck, 1993; Makeev et al., 2019 and references cited therein).

Solutions of (11) and (12) are shown in Figs. 2 and 3. In Fig. 2, two different mismatches ρ_{ML} are considered: they represent two different regimes for the wrinkling onset of fiber-reinforced bilayers. Indeed, up until the elastic mismatch between the film and the matrix is quite high (approximately $\rho_{ML} \leq 10^{-4}$), in the case of effective contribution to the substrate's overall stiffness of compressed fibers, the critical strain and the wavenumber exhibit a symmetric trend with respect to $\theta = 45°$ (see Fig. 2(a)). On the other hand, when this mismatch becomes much lower than before, as for $\rho_{ML} \geq 10^{-2}$, such symmetry is broken, leading to the curves in Fig. 2 (b). These show two peaks with different heights, approximately at 20° and 70°. It is worth noting that the elastic mismatch revealing the onset of symmetry-breaking is of the order of 10^{-3}. On the other hand, by looking at Fig. 3(a) and (b), as the mismatch decreases, the minor peak gradually disappears, thereby leaving a single one. In both Fig. 2(a) and (b), the gray zone denotes what happens when contracted fibers do not contribute to the overall mechanical response of the substrate. The higher ρ_{ML} is, the wider the range of the fiber angle for which fibers undergo contraction (e.g., about ±45° for $\rho_{ML} = 5 \times 10^{-5}$). There, it is the matrix itself that governs the substrate's behavior and, hence, the system behaves like a neo-Hookean bilayer.

To complete the comparison, results obtained by modeling the film as a neo-Hookean 3D body are considered in Fig. 2 (for the sake of brevity, calculations are not shown in the paper). Looking at the plots, one can see that both formulations coincide for high mismatches, hence for very small values of ρ_{ML}, although differences emerge when the ratio ρ_{ML} increases. Indeed, with a high contribution from the fibers ($\rho_{FM} = 10$), the critical strain provided by the plate model is slightly higher than the one resulting from the 3D formulation. This difference can be explained by noting that the plate model is stiffer than the fully 3D one, as it has a more constrained kinematics, leading to higher critical strains. However, employing a reduced formulation for the plate offers several advantages. First, both models coincide over a wide range of material parameters, reducing the computational effort. Moreover, the relative simplicity induced by the reduced model highly facilitates the derivation of scaling laws.

Fig. 3 presents an analysis showing how the constitutive parameters of the bilayer influence the critical strain and wavenumber. The analysis considers two values for the matrix/layer elastic mismatch ρ_{ML} (specifically $\rho_{ML} = 10^{-2}, 10^{-1}$). Fig. 3(a) and (b) show the trend of the critical quantities by keeping the fiber's dispersion (κ) constant and varying the ratio ρ_{FM}. In (a), ρ_{ML} is set at 1×10^{-2}, while in (b) ρ_{ML} is 1×10^{-1}. As previously noted, high values of ρ_{ML} lead to a more asymmetric curve trend, with peaks around $\theta = 67.5°$. These peaks are more evident for the critical strain for both mismatch values. In other words, the value of the critical strain at the onset of wrinkling gets significantly amplified by the presence of fibers in the substrate when the elastic mismatch between the

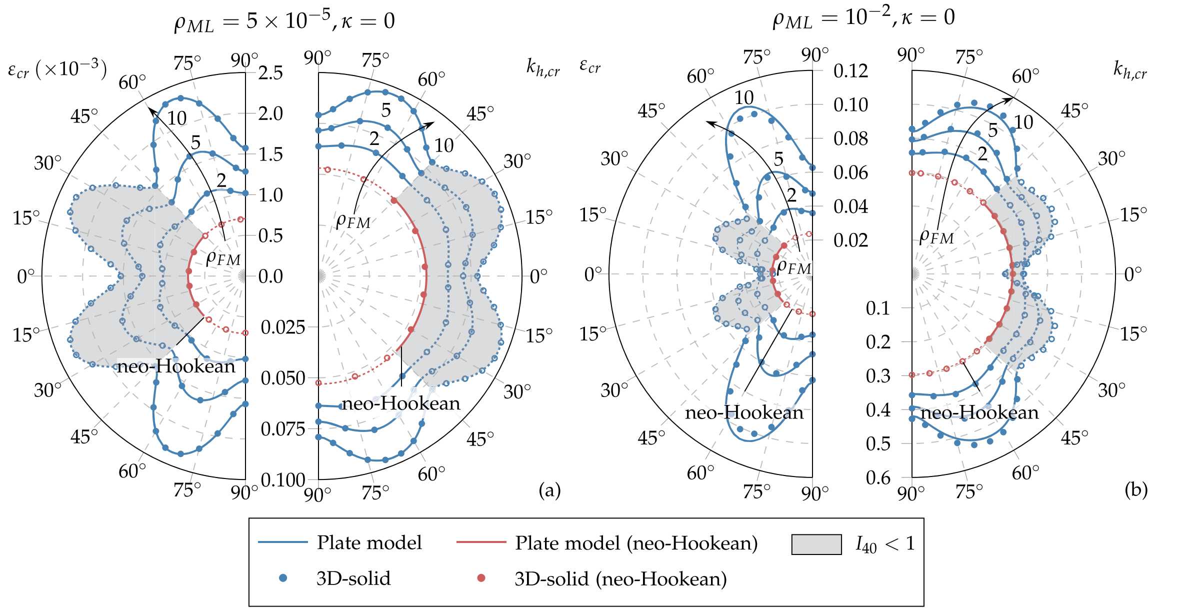

Fig. 2. Emerging *symmetry breaking* from very high-to-moderate elastic mismatches in bilayers formed by *bilateral substrates* (i.e., for which contracted fibers contribute to stiffen the resulting composite). *When this is not the case, the gray region rules out compressed fibers* according to inequality (13). In these, and in the following figures, to make the trends and the simmetries more evident, a polar representation of the critical quantities has been adopted, in which a given angle θ corresponds to a bilayer with fiber families oriented along $\pm\theta$. Comparison between the critical strain obtained from the plate model (solid line) and the 3D-solid model (dots), both for SRM substrates, with respect to the fiber angle θ, and considering three values of ρ_{FM}. In particular, the values of ρ_{FM} are consistent with those used in Nguyen et al. (2020). Two representative values of the matrix-layer elastic mismatch ρ_{ML} are chosen to show the symmetry breaking in terms of critical strain and wavenumber as functions of the fiber's orientation. For high layer-matrix mismatches, i.e., very low values of ρ_{ML}, namely $\rho_{ML} = 5 \times 10^{-5}$ in (a), the trend is symmetric with respect to $\theta = \pm 45°$. In contrast, even when compressed fibers contribute to the effective mechanical response of the substrate, such symmetry is broken when the stiffness of the matrix approaches that of the layer (b) (in this case $\rho_{ML} = 10^{-2}$). Both analyses are performed for highly polarized fibers, i.e., for $\kappa = 0$. It is worth noting that both the critical strain and the wavenumber exhibit a peak around $\theta = 67.5°$.

matrix and the film is in the interval $1 \times 10^{-2} \div 1 \times 10^{-1}$. Indeed, by looking at the curves for $\rho_{FM} = 2$ in Fig. 3, $\varepsilon_{cr,\max} \approx 1.7\, \varepsilon_{cr,nh}$ for $\rho_{ML} = 1 \times 10^{-2}$, while $\varepsilon_{cr,\max} \approx 3.4\, \varepsilon_{cr,nh}$ if $\rho_{ML} = 1 \times 10^{-1}$, where $\varepsilon_{cr,nh}$ indicates the critical strain that would occur in neo-Hookean bilayers with the given and same mismatch. In contrast, smaller variations are detected in the wavenumber (and the corresponding wavelength $2\pi/k_{h,cr}$). Indeed, the maximum deviation from the corresponding neo-Hookean value $k_{h,cr,nh}$ is, approximately, 26 % for $\rho_{ML} = 1 \times 10^{-2}$ and 15 % for $\rho_{ML} = 1 \times 10^{-1}$. Finally, as the stiffness mismatch between the layer and the matrix decreases (i.e., as ρ_{ML} increases), the critical strain exhibits significantly higher values even for relatively small fiber ratios ρ_{FM}. In Fig. 3 (a) and (b), the maximum critical strains are $\varepsilon_{cr,\max} \approx 4 \times 10^{-2}$ and $\varepsilon_{cr,\max} \approx 0.37$ when $\rho_{FM} = 2$, respectively.

Different dispersion responses are expected for the system at hand from modeling the film as a plate versus a 3D continuum. Nevertheless, the comparison displayed in Fig. 4 clearly shows that the wrinkling onset obtained by the former (occurring at a relatively small wavenumber) well approximates the one derived by using the latter. Upon revisiting the singularity condition (11) obtained above for the plate model, this can be recast as a fourth-order polynomial in the wavenumber, i.e.:

$$k_h^4 \mathcal{N}_{40} + k_h^3 \rho_{ML} \mathcal{N}_{31} - k_h^2 \left(\varepsilon^L \mathcal{D}_{20} - \rho_{ML} \mathcal{N}_{21}\right) - k_h \rho_{ML} \left(\varepsilon^L \mathcal{D}_{11} - \mathcal{N}_{11}\right) + \rho_{ML}^2 \mathcal{N}_{02} = 0. \tag{14}$$

A first remark arises from such an equation by considering the limiting case of $k_h \to \infty$. Eq. (14) shows that the leading term is $\mathcal{N}_{40}$ (its expression can be found in (A.19a) in supplementary, where its determining coefficients are reported in Supplementary material B). Of course, to make Eq. (14) converge, one must have $\mathcal{N}_{40} \to 0$ as $k_h \to \infty$. One can show that its corresponding limiting condition holds if and only if $\alpha_2 = \alpha_1$, which can never be fulfilled. This is clear in the case of the complete absence of fibers, where one has $\alpha_1 = 1$ and $\alpha_2 = \lambda_1^{-2}$, so that $\mathcal{N}_{40} = 0$ if and only if $\lambda_1^2 = 1$. Such a circumstance is not physically admissible, as its unique real and positive solution is $\lambda_1 = 1$, which identifies the undeformed configuration. Moreover, $k_h \to \infty$ obviously implies having an infinitely short wavelength, $\lambda \to 0$, at the onset of wrinkling. Noticeably, λ is proportional to the film thickness h (indeed $\lambda = 2\pi/k = 2\pi h/k_h$). Hence, the wavelength could achieve smaller values than the thickness h, leading to extremely high curvatures. This circumstance is definitely not covered by the plate model adopted in this paper, so a richer ansatz for the kinematics would be required to obtain a dimensionally-reduced model in order to mimic the outcomes of the fully 3D continuum approach for the film. This result is fully consistent with the fact that (14), the dispersion relation for the plate-fiber-reinforced substrate bilayer, exhibits a limiting value for k_h (depending on the material parameters ρ_{FM}, which there is taken to be equal to 2, ρ_{ML}, and θ) for the plate model is manifest in the display of Fig. 4. Such a figure shows a comparison between the dispersion relation resulting from the assumed plate model and

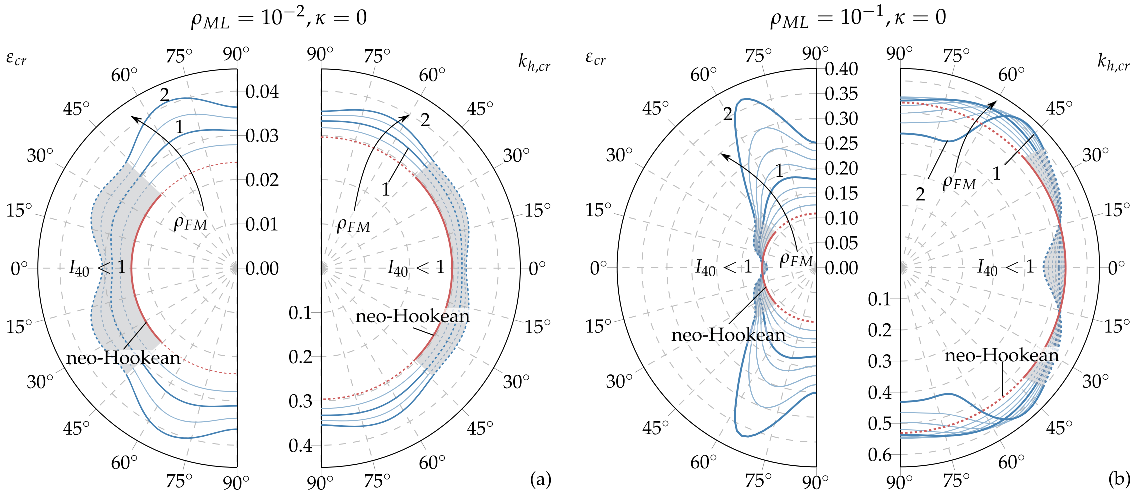

Fig. 3. Parametric analysis of the critical strain and wavenumber in moderate and medium-low mismatched bilayers. The values of the matrix-layer elastic mismatch are $\rho_{ML} = 1 \times 10^{-2}$ in (a), and $\rho_{ML} = 1 \times 10^{-1}$ in (b), respectively. No orientational dispersion is considered in this analysis ($\kappa = 0$), and $0 \leq \rho_{FM} \leq 2$. In (a) and (b), there is a peak around $\theta \approx 67.5°$ whose height is proportional to ρ_{FM}. Another local maximum is detectable for $\theta = 20°$ and $\rho_{ML} = 1 \times 10^{-2}$. When $\rho_{ML} = 1 \times 10^{-1}$, for $\theta = 20°$ such a peak becomes very minor, and this gets smoothed out as ρ_{ML} increases, i.e., when the film-matrix mismatch decreases. For $\rho_{FM} = 0$, Figures (a) and (b) show that the trend of the curves is isotropic and approaches the value of a neo-Hookean bilayer with the same mismatch ρ_{ML} (highlighted in red). Furthermore, Figure (b) shows that the fibers have a much greater effect on the critical strain than the wavenumber, with the latter being quite similar to the value reached by an analogous neo-Hookean bilayer. Of course, given the moderate to low layer-matrix mismatch, symmetry breaking of both the critical strain and wavenumber as functions of θ about $\theta = 45°$ is present in both (a) and (b). The gray color is used to represent the zone for which fibers are under contraction, i.e. the region ruled out by inequality (13).

a fully 3D modelization of the bilayer: there, the film is not described as a plate but rather as a 3D continuum. The corresponding analysis is omitted for brevity (for more details, see Appendix 1 of Nguyen et al., 2020). Looking at Fig. 4, the dispersion relation (14) is displayed for the selected set of parameters in terms of (i) the imposed strain, ε^L, and (ii) the dimensionless wavenumber k_h. This comparison shows that modeling the film as a thin plate within the bilayer limits such a model to be meaningful over a bounded set of wavenumbers. On the contrary, the corresponding fully 3D model is well-defined throughout the non-negative real axis. In particular, the data utilized in Fig. 4 for the comparison between the two models mentioned above are $\rho_{ML} = 5 \times 10^{-2}$, 1×10^{-1}, $\kappa = 0$ and $\theta = 50°, 70°$. For a given wavenumber, both models often return at least two possible critical stretches. Nevertheless, the minimum condition $\varepsilon^L_{,k_h} = 0$ forces the system to select just one solution, ε_{cr}, highlighted by colored dots. Note that all the dispersion curves of the 3D model in the lower part of the plot tend to the same value

$$\varepsilon_B := 1 - \lambda_B \approx 0.4563 \tag{15}$$

when $k_h \to \infty$, where

$$\lambda_B := \frac{3^{1/3}}{3}\left(2^{1/3}\left(\left(3 \times 33^{1/2} + 13\right)^{1/3} - \left(3 \times 33^{1/2} - 13\right)^{1/3}\right) - 1\right)^{1/2} \approx 0.5437 \tag{16}$$

is the well-known Biot´s stretch at the onset of contraction/compression-induced wrinkling for a homogeneous neo-Hookean half-space (Biot, 1963).

Fig. 4 also shows the behavior of the plate and the 3D model for any wavenumber. There, for different values of the matrix-to-layer elastic mismatch, the strain is proved to attain a local minimum corresponding to the very onset of wrinkling. From direct inspection of the figure just cited, *the onset of wrinkling is almost the same for the two models*. As discussed in the sequel, when it comes to characterizing such an onset, there is a striking advantage if a dimensionally reduced model is considered, from which one can, in fact, obtain an analytic and parametric set of scaling laws.

In addition to the intrinsic simplicity of the plate model relative to the 3D one, the main advantage of assuming that to analyze the corrugation of soft fiber-reinforced bilayers is to obtain asymptotic expansions of the wrinkling features at its onset without *a priori* information on the scaling of the critical quantities themselves. Indeed, here, the exponents of the power series are analytically obtained, and not inferred from already existing results. The coefficients of the resulting expansions are fully parametric in terms of the material properties and on the critical stretch itself, thus providing an operative tool applicable to any asymptotic bifurcation analyses at moderate-to-finite strains.

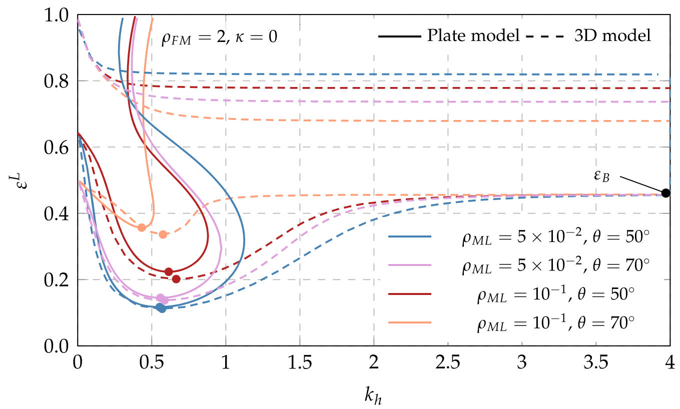

Fig. 4. Dispersion plot displaying the singularity condition yielding the critical strain for a compressed hyperelastic fiber-reinforced bilayer formed by an SRM substrate adhering to (i) a thin extensible plate and (ii) a fully 3D film. *The minimum condition $\varepsilon^L_{,k_h} = 0$ selects only one strain ε_{cr}, highlighted with colored dots, thereby confirming that the onset of wrinkling is well characterized by the plate model* for the set of parameters considered for the analyses above. Note that, unlike all the other displayed cases, for which the film mediates the onset of wrinkling (this is the most common case and it is analyzed in Section 3), for $\rho_{ML} = 10^{-1}$ and $\theta = 70°$ the substrate starts governing the onset of bifurcation, almost doubling the value of the strain necessary for wrinkling to get triggered (this regime is thoroughly discussed in Section 4). For high values of wavenumber, the 3D model exhibits an asymptotic behavior, as for every curve, and one solution (on the lower part of the two-family branches displayed above) is Biot's critical strain ε_B.

3. Film-mediated wrinkling of fiber-reinforced bilayers: direct scaling laws

While studying wrinkling for virtually any film-substrate continuum, the thin layer almost invariably dominates the selection of both the critical strain, and its associated wavenumber, at which wrinkles appear. The reason for this *film-mediated regime* is that there are very high-to-medium elastic mismatches of such thin layers versus the substrate. Although authors derived scaling laws for highly mismatched flat bilayers (i.e., for $10^{-5} \leq \rho_{ML} \leq 10^{-3}$) undergoing wrinkling induced by applied compression (see, for instance, Allen, 1969; Cao and Hutchinson, 2012; Sun et al., 2011 and Vonach and Rammerstorfer, 2000), besides the results obtained in Mirandola et al. (2023) (holding for the mismatch regime just mentioned), no such relations exist for the systems studied in the present work, i.e., when the substrate is fiber-reinforced, and when there is a *medium-low stiffness mismatch between the matrix and the upper layer*, e.g. $\rho_{ML} \geq 10^{-1}$. This section describes the procedure utilized for deriving such laws even for the medium-low matrix-to-layer elastic mismatches, for which the onset of wrinkling occurs at moderate-to-large strains.

The method presented in this work offers the advantage of applicability to a broader class of bilayers with fiber-reinforced hyperelastic substrates. Indeed, the expansions are expressed in terms of the coefficients $\mathcal{N}_{\alpha\beta}$ and $\mathcal{D}_{\alpha\beta}$ introduced earlier and defined by (A.19) in supplementary, which *can be calculated for any hyperelastic constitutive law, including any one of them suitable for fiber-reinforced substrates*. The roadmap leading to the abovementioned expansions starts with the optimality condition given by Eq. (12). This amounts to a fifth-degree *algebraic* equation in the variable k_h. Although closed-form solutions are unavailable, asymptotic solutions of Eq. (12) can be provided for very small matrix-to-layer mismatch, i.e., when ρ_{ML} approaches 0. A standard way to seek asymptotic solutions is perturbation analysis, testing various candidate power series and selecting the ones leading to meaningful results. Nevertheless, the present work aims at providing a more general method to derive scaling laws. To this end, a more robust, not trial-and-error-based method is considered. This relies on *Puiseux series*, a generalization of Taylor expansions extending exponents to rational numbers. This method, applied in Supplementary material C to our problem, determines the exponents by an iterative procedure, whereas, in general, these are derived by inspection of the equation.

The fact that an extensible plate model allowing for bending has been adopted instead of the fully 3D one facilitates the step towards utilizing the abovementioned method. It is worth remarking that the key here is that (12) is *algebraic* (hence not transcendental like the one coming from the corresponding 3D formulation). Although the latter is representable in terms of exponentials, which, of course, can be written in terms of their absolutely convergent power series, the direct algebraic nature of Eq. (12) facilitates the derivation of rigorous asymptotic approximations by Puiseux series. Although one of the aims of the present work is to derive relations for moderate-to-low elastic mismatches, the asymptotic expansions reported in Supplementary material C have been performed by considering a vanishing matrix-to-layer elastic mismatch, namely a limiting condition where, overall, the substrate is much softer than the film. This choice allows for a hierarchy of scaling laws suitable to both moderate-to-low and high mismatches, obtained in Supplementary material C. For instance, the latter case recovers the scaling laws obtained by Mirandola et al. (2023), while the ones found in Allen (1969) are further retrieved for the limiting case of a neo-Hookean substrate.

Upon performing the calculations of the asymptotics as indicated in Supplementary material C , the leading term of such expansion for the critical wavenumber reads as follows:

$$k_h = \left(\frac{\mathcal{N}_{11}}{2\mathcal{N}_{40}} \rho_{ML} \right)^{1/3} + \mathcal{O}(\rho_{ML}), \tag{17}$$

where the notation for the remainder $\mathcal{O}(\rho_{ML})$ means that this has the same order of ρ_{ML} (i.e., that goes to ∞ with the same "speed" of the linear power of ρ_{ML}), $\mathcal{N}_{11}$ and $\mathcal{N}_{40}$ are defined in (A.19) in supplementary and, through the real positive eigenvalues (A.14) in supplementary, on the matrix and fiber stiffness, μ_M and ρ_{FM}, longitudinal stretch λ_1 and on the fiber angle and dispersion, θ and κ, respectively. Hence, upon replacing Eq. (17) into Eq. (C.16) in supplementary, the following consistent binomial asymptotic expression for the critical strain is found:

$$\varepsilon_{cr} = \frac{3\mathcal{N}_{40}}{\mathcal{D}_{20}}\left(\frac{\mathcal{N}_{11}}{2\mathcal{N}_{40}}\rho_{ML}\right)^{2/3} + \frac{\mathcal{N}_{21}}{\mathcal{D}_{20}}\rho_{ML} + \mathcal{O}\left(\rho_{ML}^{4/3}\right). \tag{18}$$

Unlike the monomial asymptotic expansion (17) for the wavenumber, consistency for the approximation of the expansion for ε_{cr} yields the binomial expression above for the critical strain. Both formulas depend on the mismatch between the matrix and the layer, the fiber/matrix mismatch, and the longitudinal stretch λ_1. Additionally, these relations are influenced by the spatial dispersion of the fibers κ and their mutual orientation through the angle θ. It is worth noting that *the scaling laws obtained above* hold for any hyperelastic law for the substrate and, hence, they *are suitable for direct applications to the case at hand*.

Further simplified convergent Taylor's expansions of (17) and (18) can be obtained for (i) the case of "weak reinforcements", namely when the concentration mediated fiber-to-matrix elastic mismatch, ρ_{FM}, is not too high, and (ii) for small to moderate stretches, i.e., for λ_1 close to 1. The outcomes of such expansions read as follows:

$$k_h = \left(\Lambda_k \rho_{ML}\right)^{1/3} + \mathcal{O}\left(\rho_{ML}, \rho_{FM}^{1/2}, \lambda_1^2(\lambda_1-1)^{1/2}\right) \tag{19}$$

$$\varepsilon_{cr} = \frac{1}{4\lambda_1^2}\left(\Lambda_k \rho_{ML}\right)^{2/3} + \frac{1-\lambda_1^2}{4\lambda_1}\rho_{ML} + \mathcal{O}\left(\rho_{ML}^{4/3}, \rho_{FM}, \lambda_1^3(\lambda_1-1)\right) \tag{20}$$

with

$$\Lambda_k := \frac{3\lambda_1^4}{2}\left(1+\lambda_1^2\right)\left(\zeta_0 + \zeta_1\left(\lambda_1-1\right) + \zeta_2\left(\lambda_1-1\right)^2\right)^{1/2}. \tag{21}$$

The influence of the fibers, as well as that of the *critical* lateral stretch λ_1, is quantified by the auxiliary functions ζ_n, where $n = 0, 1, 2$. Note that from (19) onward λ_1 is to be understood as the critical stretch, unless otherwise specified, so that Eq. (20) must be solved with respect to such a variable. The critical stretch obtained is then substituted into Eq. (19) to retrieve the critical wavenumber. Functions ζ_n can be explicitly determined by particularizing the relations above by choosing the SRM model, to get the following expressions:

$$\zeta_0 = 1 + (1-3\kappa)^2\rho_{FM} + \frac{\sin^2(4\theta)}{4}(1-3\kappa)^4\rho_{FM}^2, \tag{22a}$$

$$\begin{aligned}\zeta_1 &= 2\rho_{FM}(1-3\kappa)(4(1-\kappa)\cos(2\theta) + (1-3\kappa)\cos(4\theta)) + \\ &+ (1-3\kappa)^3\rho_{FM}^2\cos(2\theta)\Big((1-3\kappa)(\cos(2\theta)+\cos(6\theta)) - 2(1-\kappa)(\cos(4\theta)-2)\Big),\end{aligned} \tag{22b}$$

$$\begin{aligned}\zeta_2 &= 2\rho_{FM}\Big(22\kappa^2 - 20\kappa + 6 - (1-\kappa)(1-3\kappa)\cos(2\theta)\Big) + \frac{(1-3\kappa)^2}{2}\rho_{FM}^2\Big(21 + \kappa(29\kappa-46) + \\ &+ 12(1-\kappa)(1-3\kappa)\cos(2\theta) - 2(\kappa+1)(5\kappa-3)\cos(4\theta) - (1-3\kappa)\Big(14(\kappa-1)\cos(6\theta) + \\ &+ 3(1-3\kappa)\cos(8\theta)\Big)\Big).\end{aligned} \tag{22c}$$

The notation utilized in (19) and (20) for the remaining associated with the expansions above can be explained as follows. The one for the wavenumber, k_h, emphasizes the fact that while the asymptotics obtained through the Puiseux expansion in the matrix-to-layer elastic mismatch, ρ_{ML}, gives an expression of order 1 in such a parameter as a second-order term, while the function (21), modulating the scaling $\rho_{ML}^{1/3}$, is of order $\mathcal{O}\left(\rho_{FM}^{1/2}\right)$ in the concentration-mediated fibers-to-matrix mismatch. An analog procedure has been followed for the critical strain (20), determining the order of the remaining for such a quantity as stated in the equation just mentioned. More details on the scaling laws (19) and (20) are discussed in Supplementary material D, while a comparison between those, the direct Puiseux relations (17) and (18), and the exact solutions of the 3D model are displayed in Fig. D.2 in supplementary for a certain choice of parameters. If very small values for ρ_{ML} are approached, i.e., if the film is much stiffer than the substrate's matrix, the expansions above can be further simplified. In such a case $\rho_{ML} \ll 1$, hence the critical quantities become very small as well. This circumstance tantamounts to having $\lambda_1 \to 1$. Hence, the scaling laws (19), (20) converge to the ones found in Mirandola et al. (2023) for small strains, namely:

$$k_h \sim \zeta_0^{1/6}\left(3\rho_{ML}\right)^{1/3} \quad \text{and} \quad \varepsilon_{cr} \sim \zeta_0^{1/3}\frac{\left(3\rho_{ML}\right)^{2/3}}{4}, \tag{23}$$

where ζ_0 is the modulating function introduced in (22a).

Furthermore, a preliminary analysis of the scaling laws derived above is applied to a “toy model” introduced in Alawiye et al. (2019), describing a bilayer with a substrate with one family of fibers, and is presented in Supplementary material F. There, among

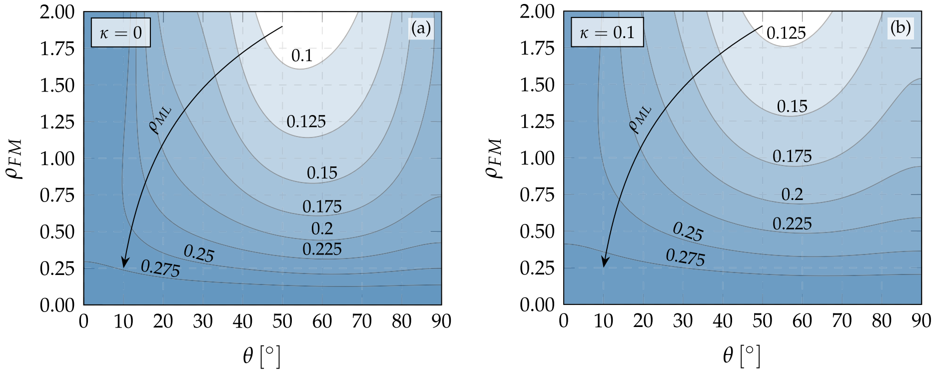

Fig. 5. Regions of validity of scaling law (26), where the discriminant $\eta_1^2 - \eta_2\eta_0 \geq 0$ for different values of ρ_{ML}, assuming $\kappa = 0$ (a) and $\kappa = 0.1$ (b).

other things, for a certain choice of parameters, the onset of wrinkling is shown to be very well approximated by the first-order self-consistent scaling law.

Although Eq. (20) should include the term in ρ_{ML} for consistency with the asymptotic expansion (19) for k_h, a truncated version involving only the first term of the expansion can be employed. This is useful for providing a more practical and prompt use of the corresponding scaling law for the critical strain, i.e.:

$$\varepsilon_{cr} = \frac{3\mathcal{N}_{40}}{\mathcal{D}_{20}}\left(\frac{\mathcal{N}_{11}}{2\mathcal{N}_{40}}\rho_{ML}\right)^{2/3} + \mathcal{O}(\rho_{ML}). \tag{24}$$

A particular case of the truncated first-order expansion (24) for the critical strain can be directly obtained by (20):

$$\varepsilon_{cr} = \frac{1}{4\lambda_1^2}\left(\Lambda_k\rho_{ML}\right)^{2/3} + \mathcal{O}(\rho_{ML}, \rho_{FM}). \tag{25}$$

Expansions (20)-(25) provide implicit relations for the critical strain at the onset of wrinkling, yet giving novel scaling laws for such quantities. The latter turn out to be in terms of the material parameters (such as ρ_{FM}) and on the stretch governing the occurrence of such an instability. Nevertheless, the following explicit scaling law for the wrinkling strain can be extracted from (20), by expanding this relation up to the second order in ε_{cr} (reminding that $\varepsilon_{cr} = 1 - \lambda_1$), and then solving for the strain and selecting the positive root:

$$\varepsilon_{cr} \sim \frac{\sqrt{\eta_1^2 - \eta_2\eta_0} - \eta_1}{\eta_2}, \tag{26}$$

where

$$\begin{aligned}
\eta_0 &= -2\zeta_0^{1/3}\left(3\rho_{ML}\right)^{2/3},\\
\eta_1 &= \frac{\zeta_0^{-2/3}}{3^{1/3}}\left(10\zeta_0 + \zeta_1\right)\rho_{ML}^{2/3} - 2\rho_{ML} + 4,\\
\eta_2 &= -\frac{2}{3^{4/3}}\zeta_0^{-5/3}\left(\zeta_0\left(38\zeta_0 + 10\zeta_1 + 3\zeta_2\right) - \zeta_1^2\right)\rho_{ML}^{2/3} + 6\rho_{ML} - 16.
\end{aligned} \tag{27}$$

Of course, in order for the critical strain to be real, the discriminant $\eta_1^2 - \eta_2\eta_0$ must be non-negative. By utilizing (22a), (22b), and (22c), η_i $(i = 0, 1, 2)$ turn out to only depend on ρ_{ML}, ρ_{FM}, κ and θ. The regions where the explicit scaling law (26) for the strain admits a positive real solution is displayed in Fig. 5. There (a) $\kappa = 0$, while in (b) the dispersion is set to 0.1. By looking at the plots, it emerges that as the matrix-to-layer mismatch ρ_{ML} increases, the admissibility of (26) reduces. Therefore, if a bilayer with a given set of parameters lies outside the admissibility region defined by Fig. 5, the explicit scaling law (26) cannot be used and, hence, either the implicit relation (20) or its truncated monomial variant (25) must be utilized instead (as in the figures of Section 4). However, the fiber dispersion κ has a beneficial effect on the validity of Eq. (26) as, for a fixed ρ_{ML}, the region for which the explicit scaling law admits a real solution increases. Finally, it is worth noting that approximation (26) retrieves $(23)_\mathrm{b}$ when $\rho_{ML} \ll 1$.

Although the asymptotic expressions above are directly obtained from the plate-substrate model, it is of great interest to compare the obtained self-consistent and truncated scaling laws to the exact solution of the 3D problem. The level of precision for such an approximation has yet to be established.

To this end, Figs. 6 and 7 (with relative errors represented in Fig. H.1 and H.2 in Supplementary material H) show a comparison among the results obtained with a 3D formulation of the bilayer characterized by an SRM substrate, the first-order scaling laws (19)-(20), and the explicit expansion (26). To this end, two different values for the matrix/layer mismatch have been considered: in Fig. 6 $\rho_{ML} = 1 \times 10^{-2}$, while in Fig. 7 $\rho_{ML} = 1 \times 10^{-1}$. Along with every comparison shown in Figs. 6 and 7 (a) and (b), the relative error is computed with respect to the 3D SRM model. The black lines and dots represent the values of a neo-Hookean bilayer, in order to show the deviation from the isotropic case. It is worth reminding that, if a fiber angle lies in the zone ruled out by (13), fibers are not active (unless they are meant to support compressive loads), thus retrieving the neo-Hookean case.

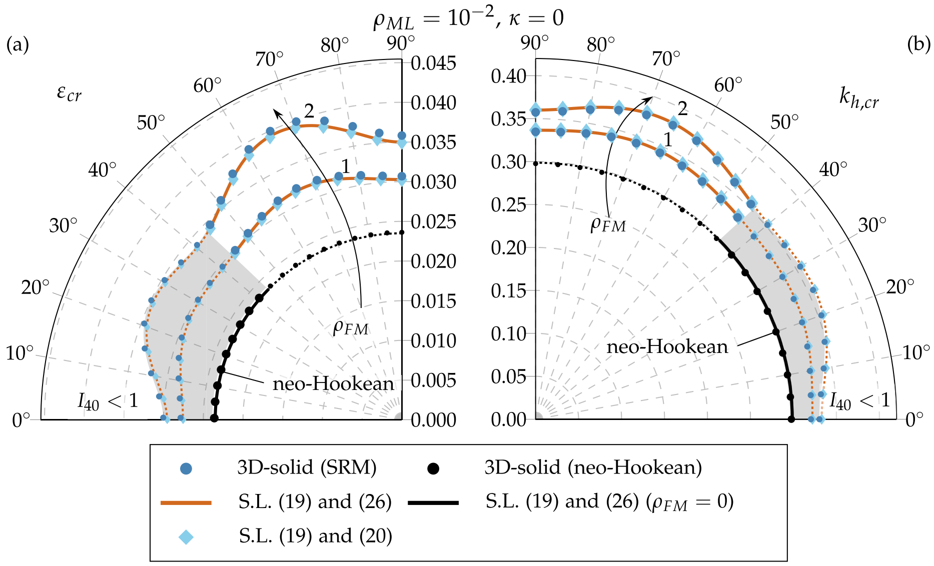

Fig. 6. Comparison between the 3D SRM model and the scaling laws (19), (20) (self-consistent) and (19), (26) (explicit). The assumed data for the bilayer are: $\rho_{ML} = 1 \times 10^{-2}$, $\kappa = 0$, and values fiber mismatches, ρ_{FM}, ranging from 0 to 2 are considered. It is worth noting that, in all the models considered here, a maximum of the critical strain and wavenumber is detected around $\theta = 67.5°$. The relative error between the wavenumber predicted by the obtained scaling laws and the exact solution for the 3D model involving the SRM response for the substrate is displayed in Fig. H.1 in supplementary. There, the good agreement of the scaling laws with the exact solution is displayed. This occurs even for moderately-reinforced bilayers, as the maximum error is about 3 % when $\rho_{FM} = 2$.

In Fig. 6 the set $\rho_{ML} = 1 \times 10^{-2}$, $\kappa = 0$ and $\rho_{FM} = 0, 1, 2$ has been chosen. In this case, both scaling laws (20)-(26) well predict the trend of the critical quantities, as the maximum error is in the order of about 3 % when $\theta \geq 65°$, even for moderate values of fiber mismatch ρ_{FM}. Noticeably, the relative error of the wavenumber is much smaller than the one recorded for the corresponding strain with both expansions. The case analyzed in Fig. 6 is representative of an artificial fiber-reinforced material, as the substrate is characterized by a perfect polarization of fibers and their contribution to the bilayer is such that they increase the critical strain by about 1.7 times that of a neo-Hookean bilayer when $\theta \approx 67.5°$.

In Fig. 7, results obtained for $\rho_{ML} = 10^{-1}$ are shown, where a minimum amount of orientational dispersion of the fibers, e.g., $\kappa = 0.1$, has been introduced. Following Holzapfel et al. (2000), for this analysis a maximum value $\rho^{\star}_{FM} := 1.573$ for ρ_{FM} is considered. The results of a parametric analysis performed by considering various materials characterized by lower values of ρ_{FM} than $\rho^{\star}_{FM}$ are shown in Fig. 7. The latter actually describes the fiber mismatch for the tunica media of the carotid artery of a rabbit. Indeed, the hyperelastic response of fiber-reinforced biological materials can be characterized through the strain energy function proposed by Holzapfel et al. (2000), Gasser et al. (2005), labeled as *OGH* in the sequel. That has a more complex form than the SRM law, as it involves an exponential term and an extra dimensionless parameter k_2, thus making the derivation of scaling laws way more challenging. Nevertheless, the use of the SRM model is justified by the fact that it is a limiting case of the law in Gasser et al. (2005) when the parameter $k_2 \to 0$ (Melnik et al., 2015). Moreover, for a certain set of material parameters, the SRM model can adequately approximate the OGH one, as shown in Fig. 7, where $k_2 = 0.8393$ has been assumed (Holzapfel et al., 2000). In this case, the maximum difference between the two formulations is about 12 % for a restricted range of fiber angles. Concerning the comparison with the scaling law, even in this scenario, the maximum relative error is acceptable, considering the self-consistent scaling law (20) and the explicit one (26). Finally, it is worth noting the behavior of the explicit scaling laws (23). As expected, they adequately describe the critical quantities when $\rho_{ML} \ll 1$, although for weakly-reinforced bilayers (see Fig. 10(a) introduced in the next section) there is almost no difference with the implicit laws of the strain (18)-(20) up to $\rho_{ML} \approx 0.3$. Moreover, explicit direct laws are completely inadequate to describe (i) moderately-to-highly reinforced bilayers and (ii) the wavenumber for any ρ_{FM}. This justifies the need for new direct scaling laws. Moreover, by looking at expressions (23), it is clear they cannot describe the asymmetric trend of Fig. 2(b), as they only depend on $\sin^2(4\theta)$. Conversely, in Supplementary material E it is shown that direct scaling laws (23) for the neo-Hookean case extend their validity toward moderate ρ_{ML}.

The analysis just developed shows that *the obtained scaling laws for the film-dominated regime apply to a wide range of elastic mismatches, from high to medium-low*, up to ρ_{ML} of the order 10^{-1}. This holds in terms of both the wavenumber and the critical strain at the onset of wrinkling, whatever the angle of reinforcement (as extensively discussed before, for lower values of such a parameter, the compressed fibers within the resulting composite contribute to stiffening and strengthening only if they operate away from failure). This allows for stating that (19), together with either (20) or its approximated form (26), *are the scaling laws for film-mediated bilayers with fiber-reinforced substrates*. Furthermore, the fact that the obtained scaling laws also apply to medium-low elastic mismatches between the thin film and the substrate renders them suitable for analyzing wrinkling in biological tissues (see, e.g., Nguyen et al.,

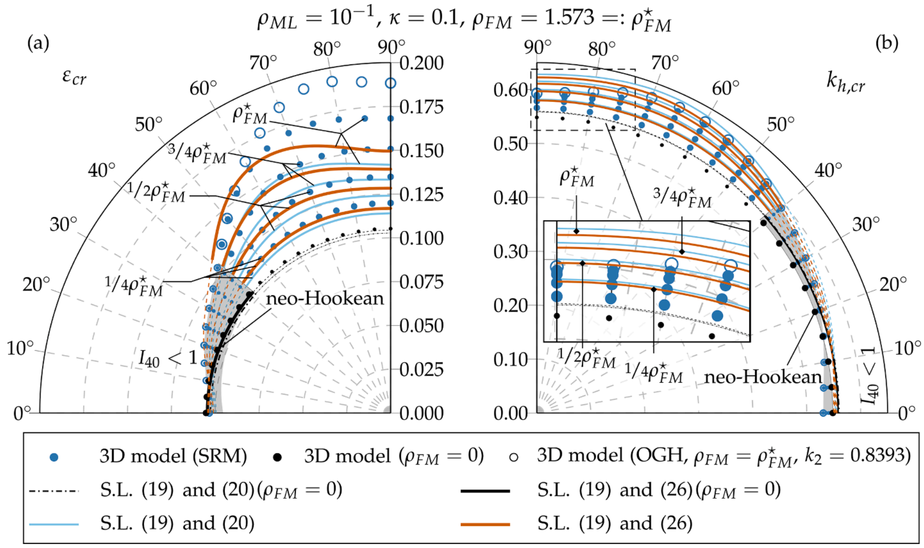

Fig. 7. Comparison between the 3D SRM model and the scaling laws (19), (20), and (26). Parameters suitable for a biological bilayer are set as follows: $\rho_{ML} = 1 \times 10^{-1}$, $\kappa = 0.1$, where the latter represents some orientational dispersion of the fibers relative to their fiber angle. The value $\rho^{\star}_{FM} := 1.573$ has been taken from Holzapfel et al. (2000). In order to compare the SRM model with the OGH law, blue circles report the results for $\rho_{FM} = \rho^{\star}_{FM}$, and $k_2 = 0.8393$ (Holzapfel et al., 2000). Relative errors with respect the 3D model are shown in Fig. H.2 in supplementary.

2020; Youn et al., 2024 for references and ad-hoc non-analytically derived scaling laws, discussed in Supplementary material I, for biological bilayers) whenever the film mediates the corrugation process.

In all existing analyses of wrinkling in layered materials—regardless of the mechanism inducing wrinkling (e.g., compression, prestretch, growth, etc.)—none of the scaling laws for fiber-reinforced bilayers reported in the literature are able to capture the behavior of bilayers with very low elastic mismatch, where the elastic modulus of the substrate matrix may be more than an order of magnitude lower than that of the film. Conversely, several studies have investigated bilayers with comparable elastic moduli in fiber-less, hence isotropic, systems using a variety of approaches, including finite element simulations and experiments (Auguste et al., 2017), as well as analyses based on 3D nonlinear elasticity and asymptotic methods (Shen et al., 2024; Jia et al., 2018; Liu et al., 2025a). In particular, the latter works further extend their analyses by incorporating the effects of growth. Of course, in such cases, the substrate's lead on wrinkling becomes substantial. Hence, a change in the regime governing the onset of wrinkling is not surprising. This suggests that, unlike the scaling laws obtained in the present section, different ones must be determined to describe the wrinkling features at its onset of very low mismatched fiber-reinforced bilayers. This circumstance will be explored in the next section for the case of externally applied compression.

4. Fiber-reinforced substrate-mediated wrinkling: isotropization and dual scaling laws

As highlighted at the end of the previous section, although the analysis performed there applies to high to medium-low mismatches, a regime change is expected to occur once the substrate's stiffness comes close to that of the layer. Preliminary analyses performed in Supplementary material E on fully isotropic, hence fiber-less, bilayers suggest that this happens when the stiffness ratio between the matrix forming the (semi-infinitely) deep substrate and the finite-thickness film ranges from a little higher than 60% to almost 100% (see Fig. E.1 in supplementary). The latter value is exact if the film is modeled as a three-dimensional body (under plane-strain conditions). On the other hand, given the limiting ratio between the depth of the substrate and the thickness of the film, for the latter is physically reasonable to assume a thin plate behavior. To this end, the extensible plate model adopted in this present work, and in many other papers, suits the inherent nonlocal behavior of such a part of the bilayer. This is due to the fact that the occurrence of curvatures (witnessing a non-local manifestation of geometrical changes of the film and of the adhering substrate's interface) is directly penalized by the plate model through its bending rigidity.

The value of matrix-to-layer elastic mismatch, ρ^{*}_{ML}, for which the regime change mentioned above occurs is expected to be significantly lower in fiber-reinforced bilayers, depending on ρ_{FM}, i.e., on the concentration and fiber´s concentration-mediated fibers-matrix elastic mismatch, and also on fiber angle, θ, and on the orientational dispersion, κ. In other words, for bilayers with slightly lower matrix-to-layer mismatches than ρ^{*}_{ML} do wrinkle through a film-substrate mediated behavior, while bilayers with slightly higher values of ρ^{*}_{ML} exhibit wrinkling primarily driven by their substrate. Such ρ^{*}_{ML} *can be viewed by the value of the mismatch for which the bilayer behaves as if it experiences a phase transition from anisotropy to effective isotropy*. We refer to such an instance by labeling it *"isotropization" of the bilayer*. This can be interpreted to be due to microstructural rearrangement of the fibers, leading to progressive overall isotropization of the mechanical response of the substrate. The limiting threshold $\rho^{\star}_{ML}$ at which the above mentioned transition occurs can be obtained by imposing the equality of the longitudinal compressive (non-spatially varying

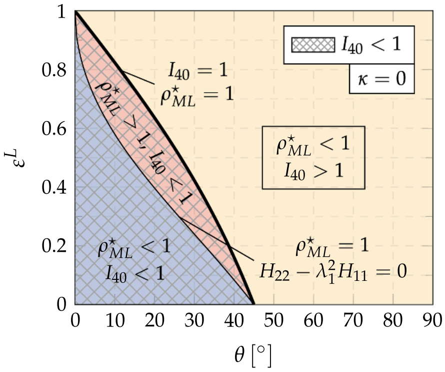

Fig. 8. Phase diagram for extended vs contracted fibers and contour plot of the transition mismatch (28) (assuming no orientational dispersion, i.e. $\kappa = 0$). From (28) follows that the sign of $\rho^\star_{ML}$ is related to the sign of $E_0(H_{22} - \lambda_1^4 H_{11})$. When this product is positive, $\rho^\star_{ML} < 1$, hence fibers lower the value of the transition mismatch. Otherwise $\rho^\star_{ML} \geq 1$. The yellow area indicates the admissibility condition (13) *and* $\rho^\star_{ML} < 1$, therefore biological materials fall within this zone: there, it is manifest that it is always the case that the regime transition between the two regimes is always set to lower values than the isotropic case, as $\rho^\star_{ML} < 1$. Note that there is only a narrow zone where fibers can defer the transition mismatch. Contracted fibers ($I_{40} < 1$) are depicted by the grid pattern.

and independent of k_h) stress component, P_{11}, arising in the substrate and in the film (modeled as a fully 3D body) right at the very onset of wrinkling. This relation yields the following expression for the sought transition threshold:

$$\rho^\star_{ML} = \frac{1}{1 + \dfrac{2\,\rho_{FM}\, E_0\big(H_{22} - \lambda_1^4\, H_{11}\big)}{1 - \lambda_1^4}}, \tag{28}$$

where E_0, H_{22} and H_{11} are reported in Supplementary material A and B. Note that Eq. (28) cannot be directly used, as the stretch at the onset of the transition is unknown. However, one can take advantage of the fact that, beyond $\rho^\star_{ML}$, the onset is almost independent of such a parameter, as shown in Fig. 10 by the blue dots, whose discussion is postponed in the second part of this section. Therefore, the critical stretch can be reasonably assumed to be the one for $\rho_{ML} \to \infty$ (vanishing film relative to the substrate), that is equivalent to solving $\mathcal{N}_{02} = 0$ for λ_1 (where $\mathcal{N}_{02}$ is defined by Eq. (A.19c) in supplementary). This equation can be easily derived by evaluating the optimality condition (12) in the limit $\rho_{ML} \to \infty$. However, further insights about the limiting case of vanishing film will be discussed in detail in a sequel paper.

Fig. 8 depicts the contour plot of the transition mismatch (28) as a function of the nominal strain ε^L and the fiber angle θ, assuming $\kappa = 0$. As $\rho_{FM} \geq 0$ and $1 - \lambda_1^4 > 0$, from (28) follows that the value of $\rho^\star_{ML}$ depends on the sign of $E_0\big(H_{22} - \lambda_1^4 H_{11}\big)$. When this product is positive, $\rho^\star_{ML} < 1$, hence fibers decrease the value of the transition mismatch. Otherwise, it is increased, i.e., $\rho^\star_{ML} > 1$. Moreover, the figure also shows the admissibility condition (13), and the excluded zones are indicated by a grid pattern. The yellow area represents the pairs (θ, ε^L) with $I_{40} > 1$ (elongated fibers) and $\rho^\star_{ML} < 1$, that is where $E_0\big(H_{22} - \lambda_1^4 H_{11}\big) > 0$. Therefore, as the fibers are not compressed, biological materials fall within this zone, so the presence of fibers always lowers the transition mismatch. Otherwise, if fibers supporting compression are assumed, the blue zone is characterized by $\rho^\star_{ML} > 1$, as well. Finally, note that there is only a narrow area where fibers defer the transition mismatch, only accessible if $I_{40} < 1$.

Fig. 8 confirms that, if $I_{40} > 1$ holds, the higher ρ_{FM} is, the lower ρ^*_{ML} becomes, thereby quantifying the extent to which the effective reinforcement yielding isotropization becomes lower than 1. The latter is recovered for $\rho_{FM} = 0$, for which $\rho^\star_{ML} = 1$. The corresponding critical strain actually emerges from the condition $\mathcal{N}_{02} = 0$, i.e., when the system is formed by the fiber-reinforced substrate alone, which is part of a separate future paper.

More insights into the behavior of mismatched bilayers can be gained by looking at their dispersion curves, characterizing the onset of wrinkling. In Fig. 9, such curves are displayed for two representative cases. Here, this is done again by modeling both the film and the substrate as fully three-dimensional continua under plane-strain conditions. Each curve corresponds to a different mismatch ρ_{ML}, and the evenly spaced range $0.3 \leq \rho_{ML} \leq 50$ has been considered. This range spans from moderate mismatches to an essentially vanishing film. Fig. 9(a) represents the dispersion of an entire family of neo-Hookean bilayers obtained by varying ρ_{ML} within the range just mentioned, while (b) shows the corresponding features of fiber-reinforced ones. The latter have been calculated by assuming $\rho_{FM} = 0.3$, $\theta = 45°$ and $\kappa = 0$. In both (a) and (b), for each ρ_{ML}, its dispersion plot presents two families of branches. This is due to the fact that (by keeping constant k_h) the determinant of the bifurcation problem has at least two real roots, and the critical strain is then obtained by the minimum condition $\varepsilon^L_{,k_h} = 0$. The neo-Hookean bilayer (see Fig. 9(a)) has minima, highlighted by red dots, at finite wavenumbers as long as $\rho_{ML} < 1$. Whenever $\rho_{ML} = 1$ is analyzed, the dispersion curve is a horizontal line at $\varepsilon^L = \varepsilon_B \approx 0.4563$, meaning that *every* wavenumber is critical, in full agreement with the standard analysis developed in Biot (1963).

By further increasing the mismatch (e.g., $1 < \rho_{ML} \leq 50$), the stationarity condition $\varepsilon^L_{,k_h} = 0$ for the contractile strain as a function of the wavenumber turns out to be verified in two cases. The first one is at small k_h, although for such a case the strain attains a local maximum. The second stationary point for ε^L is an asymptotically reached minimum at ε_B when $k_h \gg 1$, namely for a vanishing

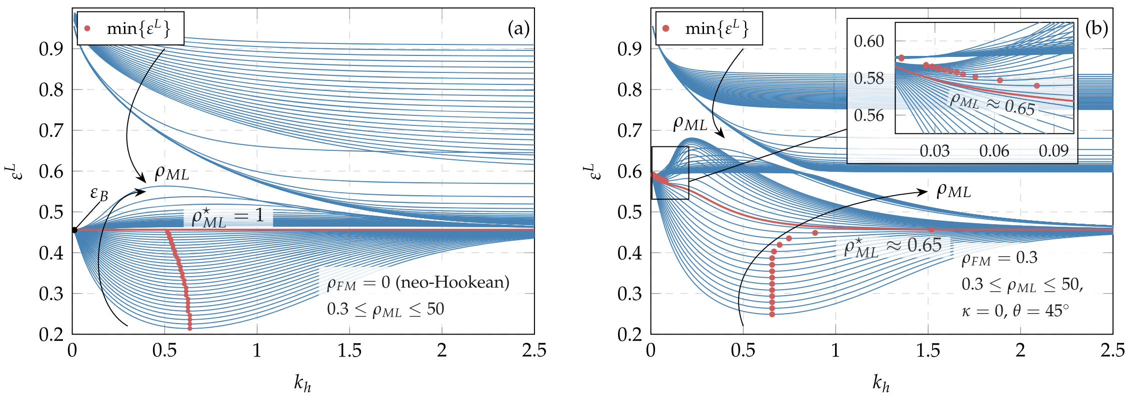

Fig. 9. Dispersion curves for fully 3D bilayers: (a) neo-Hookean system, and (b) a fiber-reinforced bilayer. Curves are generated by varying the matrix-to-layer elastic mismatch ρ_{ML}. In (a), the film has an effect on the system as long as $\rho_{ML} < 1$. For $\rho_{ML} \geq 1$, (a) shows a drastic regime change, where the substrate takes over, and the bilayer behaves like a Biot isotropic half-space. When fibers are present, (b) shows the threshold, labelled as $\rho^{\star}_{ML}$, at which the regime change occurs early. In particular, when $\rho_{ML} > \rho^{\star}_{ML}$, the wavenumber has a sudden drop, which is a manifestation of the fact that a change of regime has occurred.

wavelength. In Fig. 9(b), it is shown how fibers change the behavior of the bilayer when the mismatch reaches the threshold $\rho^{\star}_{ML}$ (for this case $\rho^{\star}_{ML} \approx 0.65$). When $\rho_{ML} < \rho^{\star}_{ML}$, the film still selects a finite wavenumber: for the range of ρ_{ML} considered here, such a finite value for the wavenumber is approximately constant. As the mismatch gets closer to $\rho^{\star}_{ML}$, the wavenumber rapidly increases and, once $\rho_{ML} = \rho^{\star}_{ML}$, k_h tends to infinity. Right after such a threshold, the wavenumber turns out to exhibit an abrupt drop and becomes very small, i.e., the bilayer manifests a drastic regime change characterized by a very large wavelength.

The natural question is to what extent an asymptotic expansion can well represent the wrinkling features across such a drastic regime change and, ultimately, deliver novel *dual scaling laws* for this case. To this end, very low mismatched bilayers are considered here to seek asymptotic expressions suited for the onset of corrugation across the regime change. The first remark one can make is that relation (11) characterizing the lateral strain, ε^L, in terms of mismatch parameter, fiber angle, and wavenumber can also be recast as follows:

$$\varepsilon^L = \frac{\mathcal{N}_{02}\lambda_h^4 + (\mathcal{N}_{11}\lambda_h^2 + \mathcal{N}_{21}\lambda_h + \mathcal{N}_{31})\lambda_h \rho_{LM} + \mathcal{N}_{40}\rho_{LM}^2}{(\mathcal{D}_{11}\lambda_h + \mathcal{D}_{20}\rho_{LM})\lambda_h^2 \rho_{LM}}, \tag{29}$$

where

$$\rho_{LM} := \rho_{ML}^{-1}, \qquad \lambda_h := k_h^{-1}, \tag{30}$$

are the elastic mismatch of the layer versus the matrix and a non-dimensional measure of the wavelength. Stationarity of this expression with respect to λ_h yields the following algebraic fifth-order equation in such a wavelength:

$$\begin{aligned}&\lambda_h^5 \mathcal{D}_{11}\mathcal{N}_{02} + 2\rho_{LM}\lambda_h^4 \mathcal{D}_{20}\mathcal{N}_{02} + \rho_{LM}\lambda_h^3\left(\rho_{LM}\mathcal{D}_{20}\mathcal{N}_{11} - \mathcal{D}_{11}\mathcal{N}_{21}\right) + \\ &\qquad - 2\rho_{LM}\lambda_h^2 \mathcal{D}_{11}\mathcal{N}_{31} - \rho_{LM}^2\lambda_h\left(\mathcal{D}_{20}\mathcal{N}_{31} + 3\mathcal{D}_{11}\mathcal{N}_{40}\right) - 2\rho_{LM}^3 \mathcal{D}_{20}\mathcal{N}_{40} = 0.\end{aligned} \tag{31}$$

Following the same procedure set up in Supplementary material C, for $\rho_{LM} < \rho^{*-1}_{ML}$, the following scaling laws for the critical strain and non-dimensional wavelength are obtained:

$$\varepsilon_{cr} = \frac{3\mathcal{N}_{31}^{1/3}}{4^{1/3}\mathcal{D}_{11}}\left(\frac{\mathcal{N}_{02}}{\rho_{LM}}\right)^{2/3} + \frac{\mathcal{N}_{21}}{\left(2\mathcal{N}_{31}\right)^{1/3}\mathcal{D}_{11}}\left(\frac{\mathcal{N}_{02}}{\rho_{LM}}\right)^{1/3} + \mathcal{O}\left(\rho_{LM}^0\right), \tag{32}$$

$$\lambda_{h,cr} = \left(2\mathcal{N}_{31}\right)^{1/3}\left(\frac{\rho_{LM}}{\mathcal{N}_{02}}\right)^{1/3} + \frac{\mathcal{N}_{21}}{3\left(2\mathcal{N}_{31}\right)^{1/3}}\left(\frac{\rho_{LM}}{\mathcal{N}_{02}}\right)^{2/3} + \mathcal{O}\left(\rho_{LM}\right), \tag{33}$$

where the terms appearing in such expressions can be found in (A.19a), (A.19b), (A.19c), and (A.19d) in supplementary.

It is crucial to note that, for the critical strain (32) to be finite as $\rho_{LM} \to 0$, the ratio $\rho_{LM}/\mathcal{N}_{02}$ must remain finite as well. Hence, the quantity $\mathcal{N}_{02}$ also has to approach zero at the same speed as ρ_{LM}. Furthermore, the same conclusion can be drawn by looking at (31) as $\lambda_h \to \infty$ (i.e., as $k_h \to 0$). As mentioned above, $\mathcal{N}_{02}$ is defined by Eq. (A.19c) in supplementary, which turns out to be the product of two functions ω_1 and ω_2, that read as follows:

$$\begin{aligned}\omega_1 = &-2\rho_{FM}\Big[H_{22}\Big(\big(\alpha_1\alpha_2\lambda_1^4-1\big)\big((1-3\kappa)\big(\lambda_1^4+1\big)\cos(2\theta)-(\kappa-1)\big(\lambda_1^4-1\big)\big)-\lambda_1^2E_0\big(\alpha_1^2\alpha_2^2\lambda_1^8+\\&+\lambda_1^4\big(\alpha_1^2+3\alpha_1\alpha_2+\alpha_2^2\big)-2\big)\Big)+(3\kappa-1)\lambda_1^4H_{12}\big(\alpha_1^2\lambda_1^4+1\big)\big(\alpha_2^2\lambda_1^4+1\big)\sin(2\theta)+\\&+\lambda_1^4H_{11}\big(\alpha_1\alpha_2\lambda_1^4-1\big)\big((3\kappa-1)\big(\lambda_1^4+1\big)\cos(2\theta)+(\kappa-1)\big(\lambda_1^4-1\big)-\lambda_1^2E_0\big)\Big]+\\&-\lambda_1^2\big(2-\lambda_1^4\big(\alpha_1^2+3\alpha_1\alpha_2+\alpha_2^2-1\big)-\alpha_1\alpha_2\lambda_1^8\big(1+\alpha_1\alpha_2\big)\big),\end{aligned}\tag{34a}$$

$$\omega_2 = \frac{16\pi^2\mu_M^2}{\lambda_1^4}\big(\alpha_2-\alpha_1\big)\Big(2\rho_{FM}H_{22}E_0+2(1-3\kappa)\lambda_1^2\rho_{FM}H_{12}\sin(2\theta)+1\Big).\tag{34b}$$

Further insights on expressions (32) and (33) can be gained by introducing the discrepancy, Δ, between the actual critical strain, ε_{cr}, versus the one that an isotropic (fiber-less) half-space would have (the latter is indeed the Biot's strain ε_B defined through (15)), as follows:

$$\Delta := \varepsilon_B - \varepsilon_{cr} = \lambda_{1,cr} - \lambda_B.\tag{35}$$

Of course, the critical strain is close to ε_B when ρ_{FM} is small. Preliminary asymptotic investigations on the function ω_1 appearing in (34a), and characterizing $\mathcal{N}_{02}$ appearing on (32) and (33), turn out to be useful for later developments. That quantity can be expanded around $\big(\Delta,\rho_{FM}\big)=(0,0)$ up to first order. Then, when no orientational dispersion is accounted for (when $\kappa=0$), one obtains:

$$\omega_1 = \omega_{10}+\Delta\,\omega_{11}+\mathcal{O}\big(\Delta^2,\lambda_B^4,\rho_{FM}^3\big),\tag{36}$$

where the quantities ω_{10} and ω_{11} are the constant and linear term in Δ, respectively:

$$\begin{aligned}\omega_{10} = &\,\rho_{FM}^2\sin^2\theta\left(\lambda_B^2(\cos(2\theta)+4\cos(4\theta)+4)-\frac{\sin^2\theta}{2}(8\cos(2\theta)+10\cos(4\theta)+9)\right)+\\&+\rho_{FM}\sin^2\theta\big(\lambda_B^2(10+\cos(2\theta))-2\sin^2\theta\big),\end{aligned}\tag{37a}$$

$$\begin{aligned}\omega_{11} = &\,\rho_{FM}^2\lambda_B\left(2\sin^2(\theta)(\cos(2\theta)+4\cos(4\theta)+4)-\frac{\lambda_B^2}{4}(12\cos(2\theta)-13\cos(4\theta)+\cos(8\theta)+24)\right)+\\&+12\lambda_B^3\big(1-\rho_{FM}\big)+2\lambda_B\big(\rho_{FM}\sin^2\theta(10+\cos(2\theta))-1\big),\end{aligned}\tag{37b}$$

Such preliminary expansions are particularly useful for the case of "diluted" fibers (i.e., values of ρ_{FM} near zero), for which the critical strain for the substrate alone is expected to be close to the Biot's strain ε_B in (15). It is worth recalling that Δ measures the discrepancy of the critical stretch with respect to the Biot´s one for a compressed and isotropic half-space. In this way, useful asymptotic expansions for the critical strain can be obtained by utilizing the procedure highlighted in the sequel. In particular, by taking advantage of expressions (34a) and (34b), upon substituting $\mathcal{N}_{02}=\omega_1\omega_2$ and recalling Eq. (36), (37a), and (37b), the dual second-order implicit scaling law of the strain (32) takes the following expanded form:

$$\varepsilon_{cr} = c_1\big((\omega_{10}+\Delta\,\omega_{11})\rho_{ML}\big)^{2/3}+c_2\big((\omega_{10}+\Delta\,\omega_{11})\rho_{ML}\big)^{1/3}+\mathcal{O}\big(\rho_{ML}^0,\Delta^{4/3},\rho_{FM}^2\big),\tag{38}$$

which holds whenever $\rho_{ML}>\rho_{ML}^*$, where ω_{10} and ω_{11} are defined in Eqs. (37a), (37b), and

$$c_1 := \frac{3^{2/3}}{4\lambda_B^2\big(1+\lambda_B^2\big)^{2/3}},\quad c_2 := \frac{3^{1/3}\big(1-\lambda_B^2\big)}{2\lambda_B\big(1+\lambda_B^2\big)^{4/3}}\tag{39}$$

and λ_B is the Biot's stretch determined by (16). There ω_2 (defined by (34b)) can be shown to act only as a modulation coefficient, whereas ω_1, defined by (34a), determines the critical stretch. Upon utilizing the procedure highlighted above on (33) (holding again for $\rho_{ML}>\rho_{ML}^*$), the non-dimensional wavelength takes the following form

$$\lambda_{h,cr} = c_3\big((\omega_{10}+\Delta\,\omega_{11})\rho_{ML}\big)^{-1/3}+c_4\big((\omega_{10}+\Delta\,\omega_{11})\rho_{ML}\big)^{-2/3}+\mathcal{O}\big(\rho_{ML},\Delta^{1/3},\rho_{FM}\big),\tag{40}$$

with

$$c_3 := \frac{2\big(1+\lambda_B^2\big)^{1/3}}{3^{1/3}}\quad\text{and}\quad c_4 := \frac{2\lambda_B\big(1-\lambda_B^2\big)}{3^{2/3}\big(1+\lambda_B^2\big)^{1/3}}.\tag{41}$$

It is worth noting that, although the asymptotic expressions introduced right above have been obtained by expanding around $\rho_{FM}=0$, it can be shown that they give reliable predictions for a wide range of values of ρ_{FM}, depending on ρ_{ML} (see, e.g., Figs. 10(b) and 11(b)).

In order to get the critical wavenumber $k_{h,cr}=\lambda_{h,cr}^{-1}$ and in analogy to what was found for the direct scaling laws in Section 3, the discrepancy Δ between the Biot's stretch and the critical one must be computed by solving Eq. (38).

Further simplifications in the asymptotics can be gained for $\rho_{LM}\to 0$ or, equivalently, $\rho_{ML}\to\infty$. In this case, the scaling laws (38) and (40) can be further simplified by neglecting the second-order term, thus leading to the following monomial forms:

$$\varepsilon_{cr}\sim\frac{3\mathcal{N}_{31}^{1/3}\omega_2^{2/3}}{4^{1/3}\mathcal{D}_{11}}\big(\omega_1\rho_{ML}\big)^{2/3},\quad \lambda_{h,cr}\sim\left(\frac{2\mathcal{N}_{31}}{\omega_2}\right)^{1/3}\big(\omega_1\rho_{ML}\big)^{-1/3}\tag{42}$$

and to their expanded counterparts

$$\varepsilon_{cr} \sim c_1\big((\omega_{10}+\Delta\,\omega_{11})\rho_{ML}\big)^{2/3} \quad \text{and} \quad \lambda_{h,cr} \sim c_3\big((\omega_{10}+\Delta\,\omega_{11})\rho_{ML}\big)^{-1/3}. \tag{43}$$

Reminding Δ in Eq. (35), whenever the discrepancy between the critical strain and the Biot's one is relatively small (i.e., $\Delta \ll 1$), Eq. $(43)_\mathrm{a}$ admits the following asymptotic explicit form

$$\varepsilon_{cr} \sim \varepsilon_B - 2\,\frac{\varepsilon_B^{3/2} - c_1^{3/2}\omega_{10}\rho_{ML}}{3\varepsilon_B^{1/2} + 2c_1^{3/2}\omega_{11}\rho_{ML}}, \tag{44}$$

holding for $\rho_{ML} > \rho^{*}_{ML}$, where ε_B is defined through (15). In the sequel, the analysis is completed for cases in which almost no elastic mismatch is detected between the film and the substrate's matrix, i.e., for $\rho_{ML} \to 1^{-}$. The latter condition is consistent with the fact that the range of dual regime arises only for $\rho_{ML} > \rho^{*}_{ML}$, and it is always the case that for effective fiber reinforcement $\rho^{*}_{ML} \le 1$. Noticeably, when ρ_{ML} is approaching 1 from below, the leading term in (38) is the one proportional to $\rho_{ML}^{1/3}$. Hence, the first entry on the right-hand side of such a formula scales as $\rho_{ML}^{2/3}$, and can be dropped while seeking an asymptotic approximation of the wrinkling features at its very onset near the no-mismatch zone. An analog procedure to the one applied above for obtaining (44) yields the following asymptotic approximation whenever $\rho_{ML} \to 1^{-}$:

$$\varepsilon_{cr} \sim \varepsilon_B - \frac{\varepsilon_B^{3} - c_2^{3}\,\omega_{10}\rho_{ML}}{3\,\varepsilon_B^{2} + c_2^{3}\,\omega_{11}\rho_{ML}}. \tag{45}$$

This also leads to its associated expression of the dimensionless wavelength, which reads as follows:

$$\lambda_{h,cr} \sim c_4\big((\omega_{10}+\Delta\,\omega_{11})\rho_{ML}\big)^{-2/3}. \tag{46}$$

Note that c_4 is provided by $(41)_\mathrm{b}$, and (46) is the expanded version of (33) as $\rho_{ML} \to 1^{-}$, after dropping the first term on the right-hand side.

It is worth noting that both expressions (44) and (45) tend, when $\rho_{ML} \to \infty$, to:

$$\varepsilon_{cr} \sim \varepsilon_B + \frac{\omega_{10}}{\omega_{11}}. \tag{47}$$

Therefore, when ρ_{ML} is sufficiently high, the strain rapidly converges to an asymptotic value approximated by (47). In Fig. 10, this already occurs for $\rho_{ML} \approx 2$, so beyond such a value the onset no longer depends on the mismatch ρ_{ML}, but only on the factors ω_{10} and ω_{11}. Due to the approximations of these two terms, the fractional polynomial resulting from the ratio ω_{10}/ω_{11} in (47) exhibits a singularity for a certain angle, when ρ_{FM} is greater than about 0.43: for example (when $\rho_{FM} \to \infty$) such ratio diverges at $\theta \approx 58.9°$. Therefore, the strain is overestimated if the angle of interest is close to the singular one. Conversely, for slightly-mismatched bilayers, the ratio in (44) and (45) is mitigated by the presence of finite ρ_{ML}, as shown in Fig. 11, where a good approximation towards the exact solution is achieved, although $\rho^{\star}_{FM} = 1.573$ is the concentration-mediated fiber-to-matrix mismatch. To this end, better results are achieved by neglecting the second-order term of ρ_{FM} in ω_{10} and ω_{11} when high values of ρ_{FM} *and* ρ_{ML} are assumed. Indeed, the ratio ω_{10}/ω_{11} diverges at $\theta \approx 24.1°$ when $\rho_{FM} \to \infty$, that is an angle ruled out by (13), namely if only the elongated fibers provide effective reinforcement for the substrate. Moreover, the range of angles influenced by the singularity is narrower than the one if second-order expansions in ρ_{FM} of ω_{10} and ω_{11} were adopted.

The roles of both the direct and the dual scaling laws are highlighted in the sequel for two paradigmatic cases, displayed in Fig. 10. For both such cases, the fiber angle is taken to be $\theta = 45°$, no orientational dispersion is considered, i.e., $\kappa = 0$, although two different values, 0.3 and $\rho^{\star}_{FM} = 1.573$, for the fiber reinforcement parameter ρ_{FM} are considered. Both figures confirm the occurrence of two regimes. This is the case in spite of how the film is modeled, namely either as a thin, extensible plate suitable for bending or as a 3D layer. While the latter exhibits a jump for a specific value of the elastic mismatch between matrix and layer, $\rho^{\star}_{ML} \approx 0.65$ and $\rho^{\star}_{ML} \approx 0.18$ respectively, the former smoothens such a jump (a comparison between the two figures shows that the stiffer the substrate is, the higher the steepening is). Unlike the 3D continuum, the smoothening is obviously due to the fact that the plate model is inherently nonlocal. Indeed, besides accounting for the extension of the layer, the occurrence of the curvature changes during wrinkling of the film perfectly bonded to the substrate is directly penalized in the assumed thin plate model. In terms of the numerical values for $\rho^{\star}_{ML}$ for the two cases examined above, it is worth mentioning that they have been evaluated by replacing the stretch arising at the right limit of the transition mismatch into (28). However, by using the asymptotic stretch obtained for $\rho_{ML} \to \infty$ by solving $\mathcal{N}_{02} = 0$ for λ_1, one gets $\rho^{\star}_{ML,\mathrm{approx}} \approx 0.62$ and $\rho^{\star}_{ML,\mathrm{approx}} \approx 0.14$, thus justifying the use of the asymptotic stretch in place of the exact one at the isotropization condition.

One notes that, no matter which model is chosen, overall dual scaling laws capture the behavior of the bilayer after the jump arising in the results from the 3D model. As it was highlighted before, this typically occurs for low matrix-to-layer elastic mismatches. On the other hand, the original asymptotics deduced in Section 3, in its various forms, predicts the critical strain at the onset of wrinkling for high to medium-low mismatched fiber-reinforced bilayers. This is consistent with the existence of ρ^{*}_{ML} that can be viewed by the value of the mismatch for which the bilayer behaves as if it experiences a phase transition between two separate regimes. Indeed, the smaller this value gets, the wider the dual regime becomes. Therefore, the validity range of the direct and dual scaling laws strongly depends on the angle of the fibers and their overall contribution to the effective reinforcement of the bilayer, as emphasized by (28). The simple calculation of $\rho^{\star}_{ML}$ directly permits one to understand which scaling, either direct or dual, one needs to apply for the case at hand.

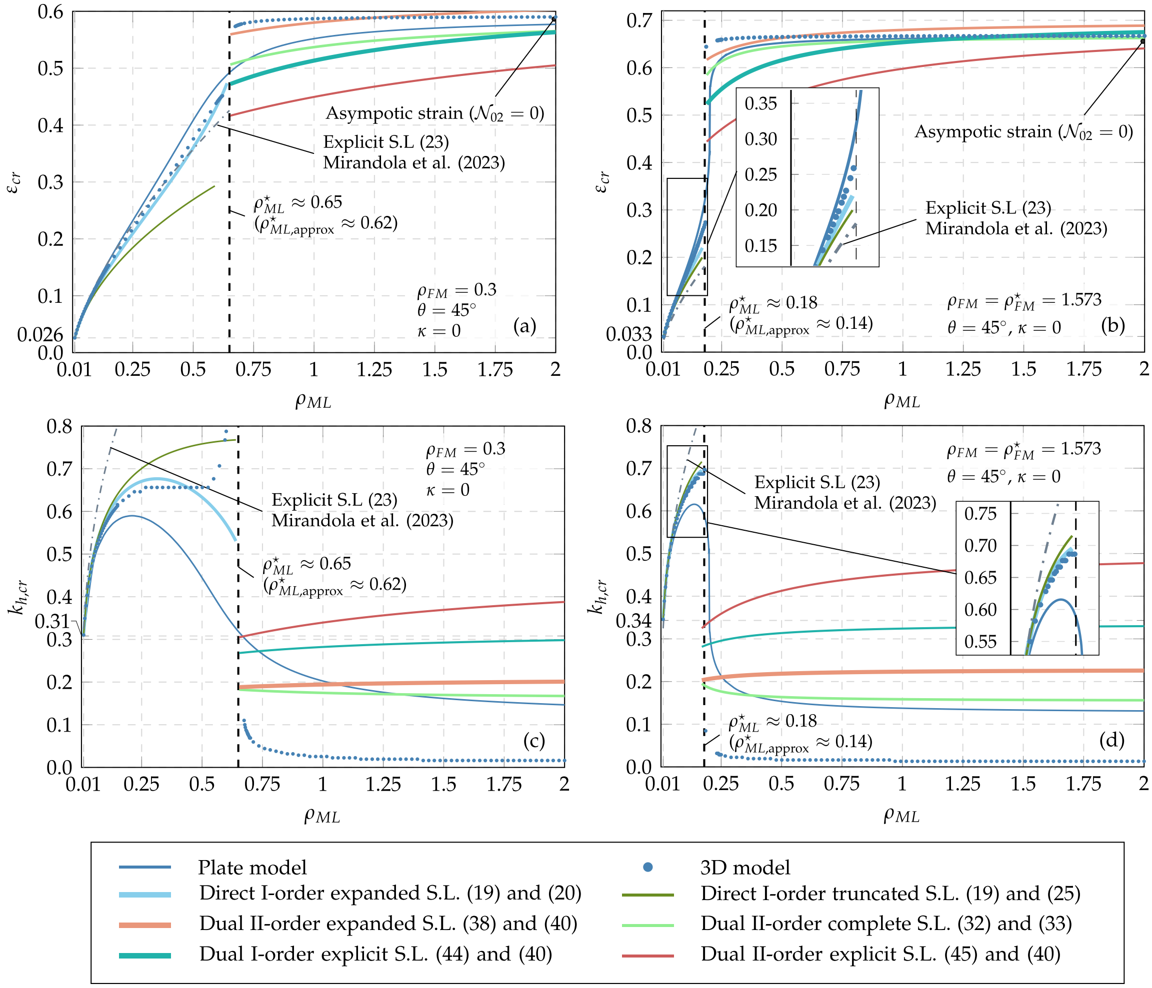

Fig. 10. Critical strain and wavenumber of a bilayer by varying the elastic mismatch ρ_{ML}. Two different values of ρ_{FM} are considered, i.e., $\rho_{FM} = 0.3$ and $\rho_{FM} = \rho^\star_{FM}$, assuming $\theta = 45°$ and no fiber dispersion (fibers are not contracted here, as they operate in the yellow region of the phase diagram displayed in Fig. 8). In both cases, an isotropization of the bilayer occurs at a threshold $\rho^\star_{ML}$ defined by Eq. (28), by using the stretch at the right limit of such a value. However, the asymptotic stretch can be used in place of the exact one for evaluating the transition mismatch, thus returning $\rho^\star_{ML,\text{approx}}$. Moreover, comparisons with direct and dual scaling laws have been made. Unless specified otherwise, the asymptotic wavenumbers are determined using the strain provided by the expansion indicated in the corresponding legend entry. Note that the zone ruled out by Eq. (13) is not represented because the fibers are not active for $\theta = 45°$ only when $\epsilon_{cr} = 0$. For the cases at hand, sharing the same fiber angle $\theta = 45°$, for the asymptotic expansion of ϵ_{cr} the green line is closest to the one corresponding to the exact solutions of both the plate and the 3D model, while the orange one for $k_{h,cr}$ turns out to be the best approximation to the outcomes of the plate model. Note that (b) and (d) have been obtained by considering the first-order expansions in ρ_{FM} of ω_{10} and ω_{11}, in order to compensate for the overestimation of the critical strain due to the high value of ρ_{FM} and ρ_{ML}.

It is also worth noting that, for instance, for both cases in Fig. 10, and for sufficiently high values of ρ_{ML}, the critical strain evaluated from the plate model and the one calculated from its corresponding (dual) scaling law asymptotically converge to the value predicted by the 3D model. Of course, the more compliant the bilayer (e.g., Fig. 10(a)), the larger the value of ρ_{ML} required to achieve the convergence just cited. For the reason previously discussed, the dual expansions in Fig. 10(b) and (d) have been obtained by considering the first-order expansions in ρ_{FM} of ω_{10} and ω_{11}, in order to compensate the overestimation of the critical strain due to the high value of ρ_{FM} and ρ_{ML}.

A final remark is due about the particular value ρ^*_{ML} of the layer-to-substrate elastic mismatch separating the behavioral regimes extensively discussed above, namely the "threshold mismatch". This obviously strongly depends on the constitutive properties of the substrate, hence on both the elastic moduli of the matrix and of the fibers, together with their concentration and orientation. To this end, Fig. 11 (with relative errors in Fig. H.4 in Supplementary material H) extends the analysis of Fig. 10(b) by varying the fiber angle θ, and considering $\rho^\star_{ML} = 0.18$ as elastic mismatch. For the sake of illustration, the latter value is chosen in such a way that the regime transition occurs at an angle, labeled as $\theta^\star$, in the interval $(45°, 50°)$. Fig. 11 clearly identifies two regimes, starting from $\theta^\star \sim 48°$. It is also confirmed that the plate model does not have such a sharp transition as in the 3D one. When the fiber angle, θ,

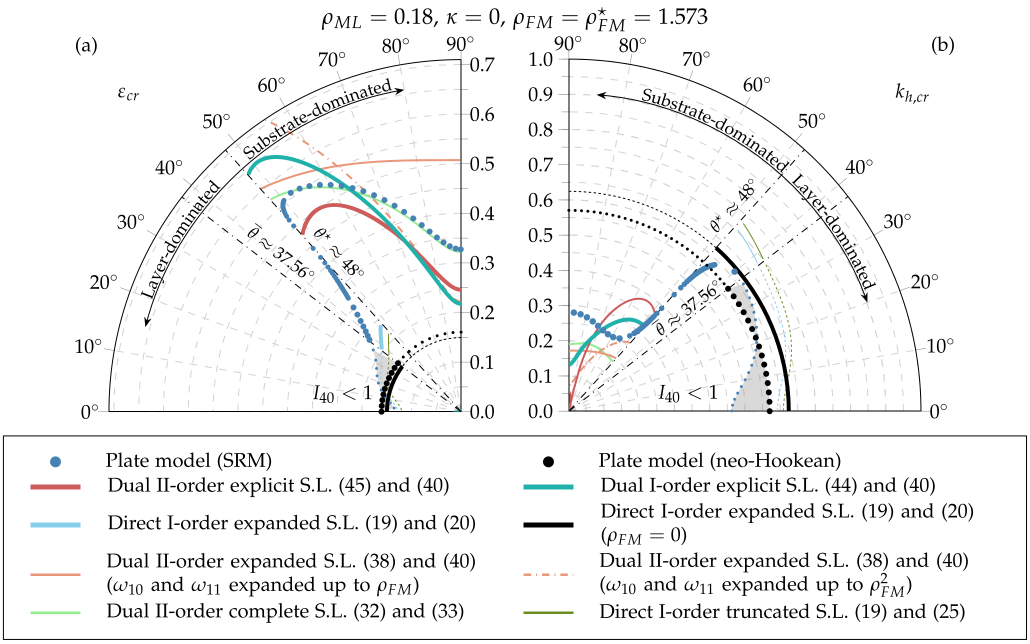

Fig. 11. Critical strain and wavenumber of a bilayer by varying the fiber angle, assuming $\rho_{ML} = \rho^{*}_{ML} = 0.18$, $\rho^{\star}_{FM}$, and $\kappa = 0$. Fibers turn out to be elongated only for angles $\theta > \bar{\theta}$, where $\bar{\theta} \approx 37.56°$ marks the gray zone of compressed reinforcement (the latter is obviously efficient if far from failure). A transition occurs around $\theta^{\star} \sim 48°$ (the angle is slightly higher than 45°, which is the value characterizing the fibers in Fig. 10(b)-(d)). The angles $\theta^{\star}$ and $\bar{\theta}$ split the domain into three regions. In particular, the two regions to be introduced are (i) $\bar{\theta} \leq \theta < \theta^{\star}$ for which the wrinkling onset is film-mediated, although with a clear increasing steepening while approaching $\theta^{\star}$ (the fully 3D model would exhibit a marked strain jump at such an angle, as displayed in Fig. 10 for a slightly different set of parameters), and (ii) $\theta > \theta^{\star}$, for which such an the onset turns out to be substrate-governed. While in the former case the corrugation features scale according to the dual asymptotics, in the latter one they obey the direct scaling laws. Relative errors with respect to the plate model are shown in Fig. H.4 in supplementary.

is such that $\theta > \theta^{\star}$, the substrate prevails in mediating the wrinkling onset of the bilayer. Therefore, right at the regime's transition, such a continuum exhibits a sudden drop of the critical wavenumber (in other words, the wavelength increases) and, for increasing values of ρ_{ML}, asymptotically tends to the critical strain given by solving $\mathcal{N}_{02} = 0$. In this case, dual scaling laws have to be utilized.

The opposite scenario occurs when $\theta < \theta^{\star}$: the film selects a finite wavenumber, together with a smaller critical strain, and the wrinkling features at its onset scale according to the laws found in Section 3.

In summary, for the *substrate-mediated regime*, besides the *complete scaling law* of the strain (32) which is obviously the most accurate one for the for the critical strain, its *two explicit versions*, i.e. (44) and (45), turn out to be appropriate to deliver upfront the order of magnitude of the strain and its angular dependence (see, e.g., Figs. 11, 12). Concerning the scaling law for the wavenumber, the lowest mean error is obtained by adopting the inverse of the expansion (40), fed with the critical stretch provided by (44).

In Fig. 12 (with relative errors displayed in Fig. H.5 in Supplementary material H), the trend of a low-mismatched bilayer with a diluted concentration of fibers is shown by assuming $\rho_{ML} = 2$ and $\rho_{FM} = 0.3$. As it turns out, unlike the cases displayed in Fig. 11, no matter what fiber angle is considered, the resulting bilayers are all in the dual regime. For the sake of illustration, a perfect alignment $\kappa = 0$ is considered. By looking at the critical strain of the plate model for such a case, one can see that the complete dual II-order scaling law (32) almost overlaps the exact solution, whereas its first-order version (42) is a lower bound. It is also not surprising that if one considers a completely film-less case, i.e., where only the fiber-reinforced substrates are present, the wrinkling strain for such a case practically overlaps with the plate solution, obviously indicating that the film in the latter case has no structural contribution to the bilayer. Indeed, unlike the pure substrate case, the thin layer here has solely a functional role. In particular, this yields a specific value of the wavelength (and of the corresponding wavenumber).

Further remarks can be drawn by looking at their variants, namely relations (38), $(42)_{\mathrm{a}}$, (44), and (45) for the critical strain, and their related formulas for the wavelength. Note that $(43)_{\mathrm{a}}$ is not represented as it is almost coincident with Eq. (44). The first worth noting result is that the scaling law for the wrinkling strain obtained by the expanded and explicit relation (44) minimizes the pointwise gap with respect to the exact (plate) solution if compared to the first-order complete expansion $(42)_{\mathrm{a}}$. This is due to the fact that the former expression is derived under the hypothesis that the discrepancy, Δ, between the critical strain at the onset of corrugation and the Biot's one (i.e., $\varepsilon_B \approx 0.4563$) is such that $\Delta \ll 1$. Naturally, this forces the wrinkling strain to have a limited deviation from such a value for most of the composites at hand. Indeed, some exceptions arise for the ones containing fibers whose angles $\theta < 20°$, for which the relative error is greater than 10 %.

Fig. 12(a) shows that Eq. (44) (obtained by expanding the first entry on the right-hand side of (38) near $\rho_{ML} \to \infty$) *is the best compromise among all the other choices to represent the critical strain in low-mismatched and substrate-dominant bilayers*. Furthermore,

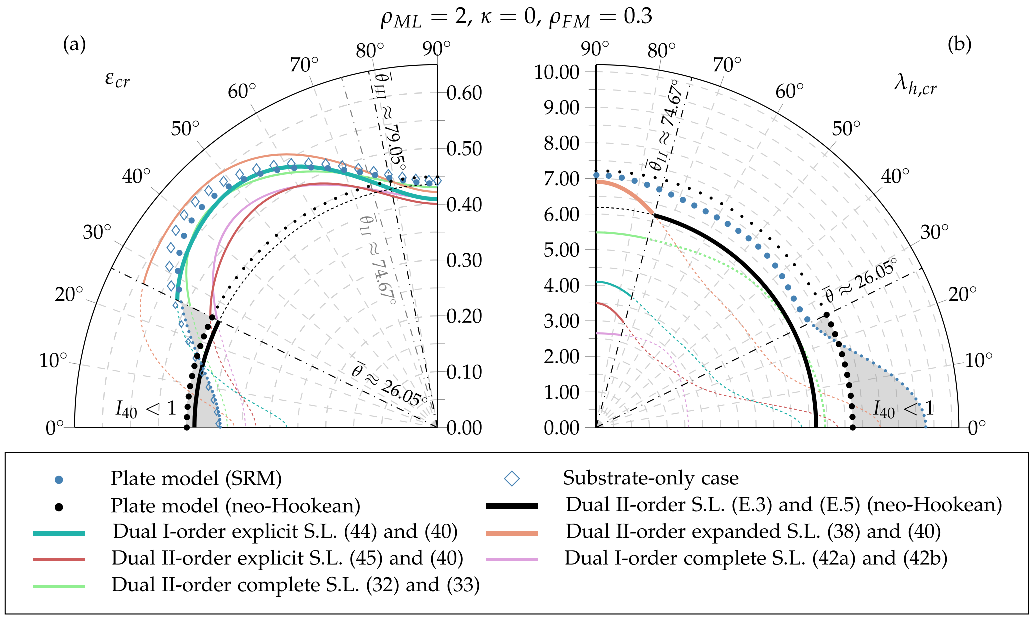

Fig. 12. Comparison of the critical strain and wavenumber of a low-mismatched bilayer, with $\rho_{ML} = 2$, $\rho_{FM} = 0.3$ and $\kappa = 0$. The expanded second-order scaling law (38) and the complete first-order one (42) form an upper and lower bound of the critical strain. The best compromise to describe ε_{cr} is the explicit law (44), as its mean error is below 5 %. On the other hand, the wavenumber is not described with the same accuracy by the dual scaling laws, as the asymptotic wavenumber overestimates that provided by the plate model when ρ_{ML} is high. On the other hand, in terms of wavelength, the scaling law characterizing the deformation mode remains almost insensitive to the presence of the fibers (the bold black line indicates that $\lambda_{h,cr}$ is closer to (E.5) in supplementary than (40)) up to the transition angle $\bar{\theta}_{II} \approx 74.67°$, at which the wavelength starts increasing. It is only at $\bar{\theta}_{III} \approx 79.05°$ that the wrinkling strain becomes lower than the value that a fully neo-Hookean substrate would exhibit, thereby enhancing the onset of corrugation to slightly lower strains than the ones of the corresponding isotropic case. On the contrary, substrates characterized by fiber angles in the interval $\bar{\theta} \le \theta < \bar{\theta}_{III}$ defer the occurrence of the onset of bifurcation which, within the subinterval $\bar{\theta} \le \theta < \bar{\theta}_{II}$ occurs essentially at constant wavelength. Relative errors with respect to the plate model are shown in Fig. H.5 in supplementary. Note that Eq. (46) is not represented in (a) because it deviates too much from the target values (see Supplementary material E for a qualitative motivation).

unlike those choices, this has the obvious advantage of being explicit and, hence, directly applicable to the problem at hand. This indeed shows an overall good agreement for all the angles, making it the best choice, as the mean relative error is below 5 %. Fig. 12(a), though, clearly confirms that the scaling law (44) remains very reliable for almost all angles whenever the bilayer's corrugation arises in the substrate-mediated regime.

A completely different scenario is detected for the scaling laws relative to the wavelength, $\lambda_{h,cr}$. Unlike the ones for the critical strain just analyzed, Fig. 12(b) shows that the scaling laws obtained for $\lambda_{h,cr}$ are essentially unable to get close to the exact solution for this quantity. The reason primarily lies in the nature of the scaling (33): in a substrate-dominated bilayer $\rho_{LM} \to 0$, so that, according to (33), even the critical wavelength must tend to zero. In such a case, the corresponding wavenumber diverges to infinity and, therefore, the scaling laws (33) and (40) overestimate the critical wavenumbers. This is shown in Fig. 12(a), as $\rho_{ML} = 2$ (i.e., $\rho_{LM} = 1/2$). An analytic proof of why scaling laws of wavenumber fail is carried out in Supplementary material E, by considering a neo-Hookean bilayer as an example. Nevertheless, by employing the *expanded binomial expansion* (40) *along with the strains provided by its paired expansion* (38), one can get the order of magnitude of the wavelength. Note that feeding the wavelength expansion with the strain given by (45) or (44) yields inaccurate results. In summary, by considering both accuracy and simplicity, *the critical strain in the dual regime scales like* Eq. (44), while *the wavelength* λ_h scales like the relation (40) (when the critical strains are provided by Eq. (38)), although with less accuracy.

5. Conclusions

Scaling laws for the critical wrinkling strain and corresponding wavenumber have long been pursued for elastically mismatched bilayers. These laws aim to relate wrinkling features directly to governing parameters, enabling efficient and reasonably accurate analysis without resorting to finite element simulations or full analytical solutions of the underlying boundary value problem. Besides a few exceptions though (e.g., Stewart et al., 2016; Nguyen et al., 2020; Mirandola et al., 2023; Montanari et al., 2024; Liu et al., 2025b), up to now the vast majority of studies have focused on bilayers with isotropic substrates, leaving a gap in the understanding of scaling laws for bilayers with fiber-reinforced substrates–regardless of the elastic mismatch between the substrate matrix and the film, or the effectiveness of the reinforcement. This work aims to make a significant contribution toward bridging that gap. Under plane strain conditions, we provide the scaling laws for the wrinkling features at its onset for fiber-reinforced bilayers subjected to lateral contraction. Among the many conclusions that can be drawn from the analysis presented in this paper, the main ones can be summarized as follows:

(a) Despite assuming that the top layer, perfectly bonded onto an fiber-reinforced substrate, behaves like an extensible thin *plate* undergoing contraction and bending, we demonstrate that *predictions for the onset of wrinkling are very close to those obtained by a fully 3D analysis*; Fig. 2 displays *very satisfactory results even for moderate-to-low mismatched* (up to the order of $\rho_{ML} \sim 10^{-2}$) *fiber-reinforced bilayers*, regardless of whether fibers undergoing contraction contribute to substrate stiffening or not;
(b) While *very highly mismatched bilayers*, i.e. $\rho_{ML} < 1 \times 10^{-4}$, *in the presence of compressed fibers contributing to the effective response* (hence away from failure), *exhibit symmetry* of both the critical strain and wavenumber *relative to* $\theta = 45°$ as functions of the fiber's angle, such *symmetry is broken* for medium-to-low mismatched ones (see, e.g., Figs. 2 and 3). Such bilayers are inherently more compliant than the previous ones, and the *anisotropy of the substrate drives a very significant change in the response*;
(c) An asymptotic analysis is performed through the use of *Puiseux series*, as extensively discussed in Sections 3 and 4 (see also Supplementary material C);
(d) *Implicit scaling laws* provided by (19) and (20) parametrically characterize the wrinkling onset for *film-dominated* fiber-reinforced bilayers. An *explicit scaling law*, (26), for the critical strain is also obtained, which fairly accurately reproduces the exact solution of the 3D bifurcation problem even for medium-low matrix-to-layer elastic mismatch. The Standard Reinforcing Model—SRM—is shown to *well capture the onset of the wrinkling features* of film-mediated fiber-reinforced bilayers undergoing contraction/compression induced-corrugation, without the necessity to utilize the OGH response (see Holzapfel et al., 2000; Gasser et al., 2005) in the range of parameters at hand (see Fig. 7). The same conclusion, extended to postwrinkling, although without determining scaling laws for the onset of bifurcation, can be found in Liu et al. (2025b);
(e) A clear *regime transition* in the wrinkling mechanism at its onset is identified when the *substrate* begins to *govern* the response of the fiber-reinforced bilayer under compression. In the absence of fibers, this transition coincides with vanishing elastic mismatch between film and substrate matrix, and occurs without strain discontinuity. Fiber reinforcement is shown to drastically modify this behavior, thereby reducing the *transition threshold* by an order of magnitude relative to the fiber-less case. Beyond this threshold, the wrinkling onset becomes *substrate-dominated* and the bilayer responds as an *effective isotropic medium* at the prescribed level of reinforcement (see Fig. 10). This transition places the substrate-dominated regime outside the range of validity of the scaling laws of Section 3, motivating the asymptotic expansions developed in Section 4 to describe the resulting dual-regime behavior;
(f) Starting from expressions (38), (40) resulting from the dilute approximation of the Puiseux relations (32) and (33), *two explicit scaling laws for the critical strain*, (44) *and* (45), have further been provided for the *dual regime*.

In summary, *the obtained scaling laws* characterizing the onset of wrinkling for fiber-reinforced bilayers *can be applied whatever the range of values of matrix-layer elastic mismatch and the effectiveness of the fiber-reinforcement* (both when this is provided by the extended fibers only or for cases in which even contracted fibers away from failure do so), as long as the regime, *film-mediated (direct)* or *substrate-guided (dual)*, at which the onset of wrinkling occurs is identified.

Future developments are foreseen in various directions. Certainly, the experimental validation of the scaling laws obtained in this present paper is of great interest for both high-to-low mismatched multimaterial-engineered fiber-reinforced bilayers at different values of fiber reinforcement, as well as for biological collagen-reinforced layered tissues. Another direction of investigation is foreseen for cases in which, alternatively, the film is fiber-reinforced and not the substrate or both of them are. The methodology introduced in this present paper can be applied to both circumstances, provided the identification of the occurring regimes arising in those enriched bilayered systems. Generalizations of the scaling laws obtained in this present work are also under investigation for the cases of both growth and prestress.

CRediT authorship contribution statement

Andrea Mirandola: Writing – review & editing, Visualization, Validation, Software, Methodology, Investigation, Formal analysis, Conceptualization; **Angelo R. Carotenuto:** Writing – review & editing, Validation, Supervision, Software, Resources, Methodology, Investigation, Funding acquisition, Formal analysis, Conceptualization; **Arsenio Cutolo:** Writing – review & editing, Validation, Supervision, Software, Resources, Methodology, Investigation, Funding acquisition, Formal analysis, Conceptualization; **Stefania Palumbo:** Writing – review & editing, Writing – original draft, Supervision, Software, Resources, Project administration, Methodology, Investigation, Funding acquisition, Formal analysis, Data curation, Conceptualization; **Massimiliano Fraldi:** Writing – review & editing, Writing – original draft, Visualization, Validation, Supervision, Resources, Methodology, Investigation, Funding acquisition, Formal analysis, Data curation, Conceptualization; **Luca Deseri:** Writing – review & editing, Writing – original draft, Visualization, Validation, Supervision, Software, Resources, Project administration, Methodology, Investigation, Funding acquisition, Formal analysis, Data curation, Conceptualization.

Data availability

Data will be made available on request.

Use of generative AI and AI-assisted technologies in the writing process

During the preparation of this manuscript, the authors utilized the software ChatGPT to partially assist them with grammatical corrections and to enhance the clarity and coherence of paragraph structures. All content was subsequently reviewed and revised by the authors, who accept full responsibility for the final version of the published article.

Declaration of competing interest

The authors declare that they have no known financial or personal conflicts of interest that could have influenced the work presented in this paper.

Acknowledgements

A.M. and L.D. gratefully acknowledge the Italian Ministry of the University and Research (MUR) in the framework of the project DICAM-EXC, Departments of Excellence 2023-2027 (grant DM 230/2022), the partial support from the grant PRIN-2022XLBLRX, and the partial financial support received by A.M. from the ERC Consolidator Grant S-FOAM, Horizon Europe EU_HE_GA 101086644, under the coordination of the P.I., Dr. Diego Misseroni.

A.M. and S.P. acknowledge the support from the Italian Ministry of University and Research within the call for proposals related to the scrolling of the final rankings of the PRIN 2022 call through the Project START (No 2022WFJ795, CUP E53C24002890001).

L.D. also gratefully acknowledges the partial support from the grant (1) SUBBIMATT Horizon Europe EU_HE_GA 101129911, (2) the ERCADG- 2021-101052956-BEYOND grant, and (3) the Italian Government through the 2023-2025 PNRR CN ICSC Spoke 7 CUP E63C22000970007 grant, awarded to the University of Trento, Italy.

S.P. also gratefully acknowledges the financial support by the National Recovery and Resilience Plan (NRRP), Mission 4, Component 2, Investment 1.1, Call for tender No. 1409 published on 14.9.2022 by the Italian Ministry of University and Research (MUR), funded by the European Union - NextGenerationEU- Project Title P2022AC8H4 MEDUSA - CUP E53D23017050001 - Grant Assignment Decree No. 1385 adopted on 1.9.2023 by the Italian Ministry of University and Research (MUR).

A.C. has been supported by the Project of National Relevance PRIN2022 grant no 2022XLBLRX funded by the Italian MUR, and he also acknowledges the financial support under the National Recovery and Resilience Plan (NRRP), Mission 4, Component 2, Investment 1.1, Call for tender No. 1409 published on 14.9.2022 by the Italian Ministry of University and Research (MUR), funded by the European Union - NextGenerationEU- Project n P2022MXCJ2 CUP E53D23018000001- Grant Assignment Decree No. 1379 adopted on 1.9.2023 by the Italian Ministry of University and Research (MUR).

A.R.C. acknowledges the financial support under the National Recovery and Resilience Plan (NRRP), Mission 4, Component 2, Investment 1.1, Call for tender No. 1409 published on 14.9.2022 by the Italian Ministry of University and Research (MUR), funded by the European Union - NextGenerationEU- Project Title P2022M3KKC MECHAVERSE - CUP E53D23017310001 - Grant Assignment Decree No. 1385 adopted on 1.9.2023 by the Italian Ministry of University and Research (MUR).

M.F. gratefully acknowledges the partial support of the Italian Ministry of the University and Research from the grant AMPHYBIA (PRIN-2022ATZCJN) and, under the complementary actions to the National Recovery and Resilience Plan, 'Fit4MedRob–Fit for Medical Robotics' Grant (PNC000007).

This manuscript was also conducted under the auspices of GNFM-INDAM.

Supplementary material

Supplementary material associated with this article can be found in the online version at 10.1016/j.jmps.2026.106564.

References

Agrawal, A., Luchette, P., Palffy-Muhoray, P., Biswal, S.L., Chapman, W.G., Verduzco, R., 2012. Surface wrinkling in liquid crystal elastomers. Soft. Matter. 8 (27), 7138–7142. https://doi.org/10.1039/C2SM25734C

Akerson, A., Elliott, R.S., 2022. Stability and post-bifurcation of film-substrate systems. Proc. R. Soc. A 478 (2264), 20220181.

Alawiye, H., Farrell, P.E., Goriely, A., 2020. Revisiting the wrinkling of elastic bilayers II: post-bifurcation analysis. J. Mech. Phys. Solids 143, 104053. https://doi.org/10.1016/j.jmps.2020.104053

Alawiye, H., Kuhl, E., Goriely, A., 2019. Revisiting the wrinkling of elastic bilayers i: linear analysis. Philos. Trans. R. Soc. A Math. Phys. Eng. Sci. 377 (2144), 20180076. https://doi.org/10.1098/rsta.2018.0076

Allen, H.G., 1969. Analysis and Design of Structural Sandwich Panels. Pergamon Press.

Alnaes, M.S., Logg, A., Ølgaard, K.B., Rognes, M.E., Wells, G.N., 2014. Unified form language: a domain-specific language for weak formulations of partial differential equations. ACM Trans. Math. Software 40. https://doi.org/10.1145/2566630

Auguste, A., Jin, L., Suo, Z., Hayward, R.C., 2017. Post-wrinkle bifurcations in elastic bilayers with modest contrast in modulus. Extreme Mech. Lett. 11, 30–36. https://doi.org/10.1016/j.eml.2016.11.013

Bae, H.J., Bae, S., Yoon, J., Park, C., Kim, K., Kwon, S., Park, W., 2017. Self-organization of maze-like structures via guided wrinkling. Sci. Adv. 3 (6), e1700071. https://doi.org/10.1126/sciadv.1700071

Balbi, V., Kuhl, E., Ciarletta, P., 2015. Morphoelastic control of gastro-intestinal organogenesis: theoretical predictions and numerical insights. J. Mech. Phys. Solids 78, 493–510. https://doi.org/10.1016/j.jmps.2015.02.016

Baratta, I.A., Dean, J.P., Dokken, J.S., Habera, M., Hale, J.S., Richardson, C.N., Rognes, M.E., Scroggs, M.W., Sime, N., Wells, G.N., 2023. DOLFINx: the next generation FEniCS problem solving environment. preprint. https://doi.org/10.5281/zenodo.10447666

Basu, S., Pollack, R., Roy, M.-F., 2006. Algorithms in Real Algebraic Geometry. Vol. 10 of *Algorithms and Computation in Mathematics*. Springer Verlag.

Ben Amar, M., 2025. Wrinkles, creases, and cusps in growing soft matter. Rev. Mod. Phys. 97 (1), 015004. https://doi.org/10.1103/RevModPhys.97.015004

Biot, M.A., 1963. Surface instability of rubber in compression. Appl. Sci. Res. Sec. A 12 (2), 168–182. https://doi.org/10.1007/BF03184638

Brau, F., Damman, P., Diamant, H., Witten, T.A., 2013. Wrinkle to fold transition: influence of the substrate response. Soft Matter. 9 (34), 8177–8186. https://doi.org/10.1039/C3SM50655J

Budday, S., Andres, S., Walter, B., Steinmann, P., Kuhl, E., 2017. Wrinkling instabilities in soft bilayered systems. Philos. Trans. R. Soc. A Math. Phys. Eng. Sci. 375 (2093), 20160163. https://doi.org/10.1098/rsta.2016.0163

Budiansky, B., Fleck, N.A., 1993. Compressive failure of fibre composites. J. Mech. Phys. Solids 41 (1), 183–211. https://doi.org/10.1016/0022-5096(93)90068-Q

Cai, Z., Fu, Y., 1999. On the imperfection sensitivity of a coated elastic half-space. Proc. R. Soc. London. Ser. A Math. Phys. Eng. Sci. 455 (1989), 3285–3309. https://doi.org/10.1098/rspa.1999.0451

Cao, Y., Hutchinson, J.W., 2012. Wrinkling phenomena in neo-hookean film/substrate bilayers. J. Appl. Mech. 79 (3), 031019. https://doi.org/10.1115/1.4005960

Cerda, E., Mahadevan, L., 2003. Geometry and physics of wrinkling. Phys. Rev. Lett. 90 (7), 074302. https://doi.org/10.1103/PhysRevLett.90.074302

Chagnon, G., Rebouah, M., Favier, D., 2015. Hyperelastic energy densities for soft biological tissues: a review. J. Elast. 120 (2), 129–160. https://doi.org/10.1007/s10659-014-9508-z

Chen, C.-M., Yang, S., 2012. Wrinkling instabilities in polymer films and their applications. Polym. Int. 61 (7), 1041–1047. https://doi.org/10.1002/pi.4223

Chen, X., Hutchinson, J.W., 2004. Herringbone buckling patterns of compressed thin films on compliant substrates. J. Appl. Mech. 71 (5), 597–603. https://doi.org/10.1115/1.1756141

Chopin, J., Démery, V., Davidovitch, B., 2015. Roadmap to the morphological instabilities of a stretched twisted ribbon. J. Elast. 119 (1), 137–189. https://doi.org/10.1007/s10659-014-9498-x

Ciarletta, P., Balbi, V., Kuhl, E., 2014. Pattern selection in growing tubular tissues. Phys. Rev. Lett. 113, 248101. https://doi.org/10.1103/PhysRevLett.113.248101

Cranston, E.D., Eita, M., Johansson, E., Netrval, J., Salajková, M., Arwin, H., Wågberg, L., 2011. Determination of Young's modulus for nanofibrillated cellulose multilayer thin films using buckling mechanics. Biomacromolecules 12 (4), 961–969. https://doi.org/10.1021/bm101330w

Cutolo, A., Pagliarulo, V., Merola, F., Coppola, S., Ferraro, P., Fraldi, M., 2020. Wrinkling prediction, formation and evolution in thin films adhering on polymeric substrata. Mater. Des. 187, 108314. https://doi.org/10.1016/j.matdes.2019.108314

Davidovitch, B., Schroll, R.D., Vella, D., Adda-Bedia, M., Cerda, E.A., 2011. Prototypical model for tensional wrinkling in thin sheets. Proc. Natl. Acad. Sci. 108 (45), 18227–18232. https://doi.org/10.1073/pnas.1108553108

De Tommasi, D., Puglisi, G., Saccomandi, G., Zurlo, G., 2010. Pull-in and wrinkling instabilities of electroactive dielectric actuators. J. Phys. D Appl. Phys. 43 (32), 325501. https://doi.org/10.1088/0022-3727/43/32/325501

Fleck, N.A., 1997. Compressive failure of fiber composites. In: Hutchinson, J.W., Wu, T.Y. (Eds.), Advances in Applied Mechanics. Elsevier. Vol. 33, pp. 43–117. https://doi.org/10.1016/S0065-2156(08)70385-5

Fu, Y.B., Ciarletta, P., 2015. Buckling of a coated elastic half-space when the coating and substrate have similar material properties. Proc. R. Soc. A 471, 20140979. https://doi.org/10.1098/rspa.2014.0979

Gasser, T.C., Ogden, R.W., Holzapfel, G.A., et al., 2005. Hyperelastic modelling of arterial layers with distributed collagen fibre orientations. J. R. Soc. Interf. 3 (6), 15–35. https://doi.org/10.1098/rsif.2005.0073

Genzer, J., Groenewold, J., 2006. Soft matter with hard skin: from skin wrinkles to templating and material characterization. Soft Matter. 2 (4), 310–323. https://doi.org/10.1039/B516741H

Georges, L., 2017. Mathematical and computational modelling of skin biophysics: a review. Proc. R. Soc. A , 47320170257. https://doi.org/10.1098/rspa.2017.0257

Gizzi, A., Cyron, C.J., Falcinelli, C., Vasta, M., 2024. Evolution of fiber distributions in homogenized constrained mixture models of soft tissue growth and remodeling: uniaxial loading. J. Mech. Phys. Solids 183, 105491. https://doi.org/10.1016/j.jmps.2023.105491

Gizzi, A., Pandolfi, A., Vasta, M., 2018. A generalized statistical approach for modeling fiber-reinforced materials. J. Eng. Math. 109 (1), 211–226. https://doi.org/10.1007/s10665-017-9943-5

Goriely, A., Mihai, L.A., 2021. Liquid crystal elastomers wrinkling. Nonlinearity 34 (8), 5599. https://doi.org/10.1088/1361-6544/ac09c1

Greaney, P., Meere, M., Zurlo, G., 2019. The out-of-plane behaviour of dielectric membranes: description of wrinkling and pull-in instabilities. J. Mech. Phys. Solids 122, 84–97. https://doi.org/10.1016/j.jmps.2018.09.006

Guo, Z.Y., Peng, X.Q., Moran, B., 2007. Mechanical response of neo-Hookean fiber reinforced incompressible nonlinearly elastic solids. Int. J. Solids Struct. 44 (6), 1949–1969. https://doi.org/10.1016/j.ijsolstr.2006.08.018

Hamzat, A.K., Murad, M.S., Adediran, I.A., Asmatulu, E., Asmatulu, R., 2025. Fiber-reinforced composites for aerospace, energy, and marine applications: an insight into failure mechanisms under chemical, thermal, oxidative, and mechanical load conditions. Adv. Compos. Hybrid Mater. 8 (1), 152. https://doi.org/10.1007/s42114-024-01192-y

Healey, T.J., 2023. An existence theorem for a class of wrinkling models for highly stretched elastic sheets. Zeitschrift für angewandte Mathematik und Physik 74, 221. https://doi.org/10.1007/s00033-023-02111-9

Hohlfeld, E., Mahadevan, L., 2011. Unfolding the sulcus. Phys. Rev. Lett. 106 (10), 105702. https://doi.org/10.1103/PhysRevLett.106.105702

Holzapfel, G.A., Gasser, T.C., Ogden, R.W., 2000. A new constitutive framework for arterial wall mechanics and a comparative study of material models. J. Elastic. Phys. Sci. Solids 61 (1), 1–48. https://doi.org/10.1023/A:1010835316564

Holzapfel, G.A., Ogden, R.W., 2017. On fiber dispersion models: exclusion of compressed fibers and spurious model comparisons. J. Elast. 129, 49–68. https://doi.org/10.1007/s10659-016-9605-2

Huang, Z.Y., Hong, W., Suo, Z., 2005. Nonlinear analyses of wrinkles in a film bonded to a compliant substrate. J. Mech. Phys. Solids 53 (9), 2101–2118. https://doi.org/10.1016/j.jmps.2005.03.007

Hutchinson, J.W., 2013. The role of nonlinear substrate elasticity in the wrinkling of thin films. Philos. Trans. R. Soc. A Math. Phys. Eng. Sci. 371 (1993), 20120422. https://doi.org/10.1098/rsta.2012.0422

Jia, F., Pearce, S., Goriely, A., 2018. Curvature delays growth-induced wrinkling. Phys. Rev. E - Stat. Nonlinear Soft Matter Phys. 98 (3). https://doi.org/10.1103/PhysRevE.98.033003

Khurana, A., Joglekar, M.M., Zurlo, G., 2022. Electromechanical stability of wrinkled dielectric elastomers. Int. J. Solids Struct. 246–247, 111613. https://doi.org/10.1016/j.ijsolstr.2022.111613

Koo, J.H., Kim, D.C., Shim, H.J., Kim, T.-H., Kim, D.-H., 2018. Flexible and stretchable smart display: materials, fabrication, device design, and system integration. Adv. Funct. Mater. 28 (35), 1801834. https://doi.org/10.1002/adfm.201801834

Kudrolli, A., Chopin, J., 2018. Tension-dependent transverse buckles and wrinkles in twisted elastic sheets. Proc. R. Soc. A , 47420180062. https://doi.org/10.1098/rspa.2018.0062

Kurashige, M., 1981. Instability of a transversely isotropic elastic slab subjected to axial loads. J. Appl. Mech. 48 (2), 351–356. https://doi.org/10.1115/1.3157621

Kurashige, M., 1983. Compressive strength of fiber-reinforced materials. Acta Mech. 49 (1), 1619–6937. https://doi.org/10.1007/BF01181754

Landis, C.M., Huang, R., Hutchinson, J.W., 2022. Formation of surface wrinkles and creases in constrained dielectric elastomers subject to electromechanical loading. J. Mech. Phys. Solids 167, 105023. https://doi.org/10.1016/j.jmps.2022.105023

Lee, G., Zarei, M., Wei, Q., Zhu, Y., Lee, S.G., 2022. Surface wrinkling for flexible and stretchable sensors. Small 18 (42), 2203491. https://doi.org/10.1002/smll.202203491

Li, L., Zheng, Y., Liu, E., Zhao, X., Yu, S., Wang, J., Han, X., Xu, F., Cao, Y., Lu, C., Gao, H., 2022. Stretchable and ultrasensitive strain sensor based on a bilayer wrinkle-microcracking mechanism. Chem. Eng. J. 437, 135399. https://doi.org/10.1016/j.cej.2022.135399

Lin, G., Li, J., Xu, Z., Ge, D., Sun, W., Chen, P., 2021. Hierarchical surface patterns via global wrinkling on curved substrate for fluid drag control. Adv. Mater. Interf. 8 (1), 2001489. https://doi.org/10.1002/admi.202001489

Liu, A., Yao, Y., Yao, J., Liu, T., 2022. Droplet spreading induced wrinkling and its use for measuring the elastic modulus of polymeric thin films. Macromolecules 55 (10), 3877–3885. https://doi.org/10.1021/acs.macromol.2c00345

Liu, H., James, R.D., et al., 2024. Design of origami structures with curved tiles between the creases. J. Mech. Phys. Solids 185, 105559. https://doi.org/10.1016/j.jmps.2024.105559

Liu, Y., 2024. Mathematics of wrinkling in three dimensional fiber reinforced bilayers. Undergoing research. Private communication at NEAT-Nonlinear elasticity and all of that-Conference in honor of Giuseppe Saccomandi sixtieth birthday, Bari, November 19–22, 2024.

Liu, Y., Goriely, A., Mihai, L.A., 2025a. Elephant trunk wrinkles: a mathematical model of function and form. Nonlinearity 38 (3), 035004. https://doi.org/10.1088/1361-6544/adaf6c

Liu, Y., Liu, R.-C., Ma, W., Goriely, A., 2025b. Post-buckling of fiber-reinforced soft tissues. J. Mech. Phys. Solids 203, 106220. https://doi.org/10.1016/j.jmps.2025.106220

Liu, Z.F., Fang, S., Moura, F.A., Ding, J.N., Jiang, N., Di, J., Zhang, M., Lepró, X., Galvão, D.S., Haines, C.S., Yuan, N.Y., Yin, S.G., Lee, D.W., Wang, R., Wang, H.Y., Lv, W., Dong, C., Zhang, R.C., Chen, M.J., Yin, Q., Chong, Y.T., Zhang, R., Wang, X., Lima, M.D., Ovalle-Robles, R., Qian, D., Lu, H., Baughman, R.H., et al., 2015. Hierarchically buckled sheath-core fibers for superelastic electronics, sensors, and muscles. Science 349 (6246), 400–404. https://doi.org/10.1126/science.aaa7952

Lu, J., He, X., Auricchio, F., 2025. A waviness-centered damage model for collagenous soft tissues. Acta Biomater. 195, 134–143. https://doi.org/10.1016/j.actbio.2025.01.031

Ma, T., Bai, J., Li, T., Chen, S., Ma, X., Yin, J., Jiang, X., 2021. Light-driven dynamic surface wrinkles for adaptive visible camouflage. Proc. Natl. Acad. Sci. 118 (48), e2114345118. https://doi.org/10.1073/pnas.2114345118

Mahadevan, L., Rica, S., 2005. Self-organized origami. Science 307 (5716), 1740–1740. https://doi.org/10.1126/science.1105169

Makeev, A., Ghaffari, S., Seon, G., 2019. Improving compressive strength of high modulus carbon-fiber reinforced polymeric composites through fiber hybridization. Int. J. Eng. Sci. 142, 145–157. https://doi.org/10.1016/j.ijengsci.2019.06.004

Mane, S., Huang, R., 2022. Rate-dependent wrinkling and subsequent bifurcations of an elastic thin film on a viscoelastic layer. Int. J. Solids Struct. 257, 111592. https://doi.org/10.1016/j.ijsolstr.2022.111592

Melnik, A.V., Borja Da Rocha, H., Goriely, A., 2015. On the modeling of fiber dispersion in fiber-reinforced elastic materials. Int. J. Non Linear Mech. 75, 92–106. https://doi.org/10.1016/j.ijnonlinmec.2014.10.006

Mirandola, A., Cutolo, A., Carotenuto, A.R., Nguyen, N., Pocivavsek, L., Fraldi, M., Deseri, L., 2023. Toward new scaling laws for wrinkling in biologically relevant fiber-reinforced bilayers. J. Appl. Phys. 134 (15), 154702. https://doi.org/10.1063/5.0161150

Montanari, M., Hamaied, R., Gao, C., Bertolin, C., Spagnoli, A., 2024. An exploration into surface wrinkling in 3D printing inspired orthotropic bilayer systems. Int. J. Solids Struct. 298, 112862. https://doi.org/10.1016/j.ijsolstr.2024.112862

Nagashima, S., Okamoto, R., Matsubara, S., Okumura, D., 2025. Soft wetting of film-substrate bilayers: wrinkle flattening near the three-phase contact line. Int. J. Multiphase Flow 191, 105324. https://doi.org/10.1016/j.ijmultiphaseflow.2025.105324

Nguyen, N., Nath, N., Deseri, L., Tzeng, E., Velankar, S.S., Pocivavsek, L., 2020. Wrinkling instabilities for biologically relevant fiber-reinforced composite materials with a case study of Neo-Hookean/Ogden–Gasser–Holzapfel bilayer. Biomech. Model. Mechanobiol. 19 (6), 2375–2395. https://doi.org/10.1007/s10237-020-01345-0

Niu, K., Talreja, R., 2000. Modeling of compressive failure in fiber reinforced composites. Int. J. Solids Struct. 37 (17), 2405–2428. https://doi.org/10.1016/S0020-7683(99)00010-4

Oguntade, E., Wigham, C., Owuor, L., Aryal, U., O'Grady, K., Acierto, A., Zha, R.H., Henderson, J.H., 2024. Dry and wet wrinkling of a silk fibroin biopolymer by a shape-memory material with insight into mechanical effects on secondary structures in the silk network. J. Mater. Chem. B 12 (26), 6351–6370. https://doi.org/10.1039/D4TB00112E

O'Kiely, D., Xin, M., Vella, D., 2025. Wrinkling of a bilayer with spatially-varying stiffness: from wrinkle branching to cascades. Proc. Ro. Soc. A 481, 20240842. https://doi.org/10.1098/rspa.2024.0842

Opelt, C.V., Cândido, G.M., Rezende, M.C., 2018. Compressive failure of fiber reinforced polymer composites - a fractographic study of the compression failure modes. Mater. Today Commun. 15, 218–227.

Pamulaparthi Venkata, S., Balbi, V., Destrade, M., Zurlo, G., 2024. Designing necks and wrinkles in inflated auxetic membranes. Int. J. Mech. Sci. 268, 109031. https://doi.org/10.1016/j.ijmecsci.2024.109031

Pandolfi, A., Vasta, M., et al., 2012. Fiber distributed hyperelastic modeling of biological tissues. Microstruc. Anisotrop. 44, 151–162. https://doi.org/10.1016/j.mechmat.2011.06.004

Pandurangi, S.S., Akerson, A., Elliott, R.S., Healey, T.J., Triantafyllidis, N., 2022. Nucleation of creases and folds in hyperelastic solids is not a local bifurcation. J. Mech. Phys. Solids 160, 104749. https://doi.org/10.1016/j.jmps.2021.104749

Pence, T.J., Song, J., 1991. Buckling instabilities in a thick elastic three-ply composite plate under thrust. Int. J. Solids Struct. 27 (14), 1809–1828. https://doi.org/10.1016/0020-7683(91)90014-7

Pitre, N., 2024. Investigation of Arterial Luminal Topography and Design of Crimped Fiber Composites. Ph.D. thesis. University of Pittsburgh. https://doi.org/10.13140/RG.2.2.27037.93924

Pocivavsek, L., Dellsy, R., Kern, A., Johnson, S., Lin, B., Lee, K. Y.C., Cerda, E., 2008. Stress and fold localization in thin elastic membranes. Science 320 (5878), 912–916. https://doi.org/10.1126/science.1154069

Pocivavsek, L., Ye, S.-H., Pugar, J., Tzeng, E., Cerda, E., Velankar, S., Wagner, W.R., 2019. Active wrinkles to drive self-cleaning: a strategy for anti-thrombotic surfaces for vascular grafts. Biomaterials 192, 226–234. https://doi.org/10.1016/j.biomaterials.2018.11.005

Poteaux, A., Rybowicz, M., 2012. Good reduction of puiseux series and applications. J. Symb. Comput. 47 (1), 32–63. https://doi.org/10.1016/j.jsc.2011.08.008

Pretti, G., Coombs, W.M., Augarde, C.E., 2022. A displacement-controlled arc-length solution scheme. Comput. Struct. 258, 106674. https://doi.org/10.1016/j.compstruc.2021.106674

Puntel, E., Deseri, L., Fried, E., 2011. Wrinkling of a stretched thin sheet. J. Elast. 105 (1), 137–170. https://doi.org/10.1007/s10659-010-9290-5

Qin, J., Yin, L.-J., Hao, Y.-N., Zhong, S.-L., Zhang, D.-L., Bi, K., Zhang, Y.-X., Zhao, Y., Dang, Z.-M., 2021. Flexible and stretchable capacitive sensors with different microstructures. Adv. Mater. 33 (34), 2008267. https://doi.org/10.1002/adma.202008267

Qiu, G.Y., Pence, T.J., 1997. Remarks on the behavior of simple directionally reinforced incompressible nonlinearly elastic solids. J. Elast. 49 (1), 1–30. https://doi.org/10.1023/A:1007410321319

Ramachandran, R.G., de Cortie, J., Maiti, S., Deseri, L., Velankar, S.S., 2021. Uniaxial stretch-release of rubber-plastic bilayers: strain-dependent transition to stable helices, rolls, saddles, and tubes. Extreme Mech. Lett. 48, 101384. https://doi.org/10.1016/j.eml.2021.101384

Robertson, A.M., Watton, P.N., 2013. Chapter 8 - mechanobiology of the arterial wall. In: Becker, S.M., Kuznetsov, A.V. (Eds.), Transport in Biological Media. Elsevier, Boston, pp. 275–347. https://doi.org/10.1016/B978-0-12-415824-5.00008-4

Federico, S., Gasser, C.T., 2010. Nonlinear elasticity of biological tissues with statistical fibre orientation. J. R. Soc. Interf. , 7955–966. https://doi.org/10.1098/rsif.2009.0502

Federico, S., Pajerski, J., Gasser, C.T., 2011. Corrigendum for the paper 'nonlinear elasticity of biological tissues with statistical fibre orientation'. J. R. Soc. Interf. , 81367–81368https://doi.org/10.1098/rsif.2011.0365

Scroggs, M.W., Baratta, I.A., Richardson, C.N., Wells, G.N., 2022a. Basix: a runtime finite element basis evaluation library. J. Open Source Softw. 7 (73), 3982. https://doi.org/10.21105/joss.03982

Scroggs, M.W., Dokken, J.S., Richardson, C.N., Wells, G.N., 2022b. Construction of arbitrary order finite element degree-of-freedom maps on polygonal and polyhedral cell meshes. ACM Trans. Math. Softw. 48 (2), 18:1–18:23. https://doi.org/10.1145/3524456

Sharma, H., Kumar, A., Rana, S., Sahoo, N.G., Jamil, M., Kumar, R., Sharma, S., Li, C., Kumar, A., Eldin, S.M., Abbas, M., 2023. Critical review on advancements on the fiber-reinforced composites: role of fiber/matrix modification on the performance of the fibrous composites. J. Mater. Res. Technol. 26, 2975–3002. https://doi.org/10.1016/j.jmrt.2023.08.036

Sharp, J.S., Thomas, K.R., Weir, M.P., 2007. Mechanically driven wrinkling instability in thin film polymer bilayers. Phys. Rev. E 75 (1), 011601. https://doi.org/10.1103/PhysRevE.75.011601

Shashwati, S., 2022. Some effects of fiber dispersion on the mechanical response of incompressible soft solids. J. Elast. 150 (1), 119–149. https://doi.org/10.1007/s10659-022-09901-8
Shen, J., Fu, Y., Pirrera, A., Groh, R. M.J., 2024. Wrinkling of differentially growing bilayers with similar film and substrate moduli. J. Mech. Phys. Solids 193, 105900. https://doi.org/10.1016/j.jmps.2024.105900
Shield, T.W., Kim, K.S., Shield, R.T., 1994. The buckling of an elastic layer bonded to an elastic substrate in plane strain. J. Appl. Mech. 61 (2), 231–235. https://doi.org/10.1115/1.2901434
Silverberg, J.L., Evans, A.A., McLeod, L., Hayward, R.C., Hull, T., Santangelo, C.D., Cohen, I., et al., 2014. Using origami design principles to fold reprogrammable mechanical metamaterials. Science 345 (6197), 647–650. https://doi.org/10.1126/science.1252876
Slaughter, W.S., Fan, J., Fleck, N.A., 1996. Dynamic compressive failure of fiber composites. J. Mech. Phys. Solids 44 (11), 1867–1890. https://doi.org/10.1016/0022-5096(96)00050-6
Song, J., Jiang, H., Liu, Z.J., Khang, D.Y., Huang, Y., Rogers, J.A., Lu, C., Koh, C.G., 2008. Buckling of a stiff thin film on a compliant substrate in large deformation. Int. J. Solids Struct. 45 (10), 3107–3121. https://doi.org/10.1016/j.ijsolstr.2008.01.023
Stewart, P.S., Waters, S.L., El Sayed, T., Vella, D., Goriely, A., 2016. Wrinkling, creasing, and folding in fiber-reinforced soft tissues. Extreme Mech. Lett. 8, 22–29. https://doi.org/10.1016/j.eml.2015.10.005
Sun, J.-Y., Xia, S., Moon, M.-W., Oh, K.H., Kim, K.-S., 2011. Folding wrinkles of a thin stiff layer on a soft substrate. Proc. R. Soc. A Math. Phys. Eng. Sci. 468 (2140), 932–953. https://doi.org/10.1098/rspa.2011.0567
Tan, A., Pellegrino, L., Ahmad, Z., Cabral, J.T., 2022. Tunable structural color with gradient and multiaxial polydimethylsiloxane wrinkling. Adv. Opt. Mater. 10 (17), 2200964. https://doi.org/10.1002/adom.202200964
Thomson, D., Cui, H., Erice, B., Petrinic, N., 2019. A study on the longitudinal compression strength of fibre reinforced composites under uniaxial and off-axis loads using cross-ply laminate specimens. Compos. Part A Appl. Sci. Manufac. 121, 213–222. https://doi.org/10.1016/j.compositesa.2019.03.034
Triantafyllidis, N., Abeyaratne, R., 1983. Instabilities of a finitely deformed fiber-reinforced elastic material. J. Appl. Mech. 50 (1), 149–156. https://doi.org/10.1115/1.3166983
Veldin, T., Trojer, J., Brank, B., Brojan, M., 2025. Wrinkling of thin plates and shells on shrinking substrates. Thin-Walled Struc. 215, 113504. https://www.sciencedirect.com/science/article/pii/S026382312500597X. https://doi.org/https://doi.org/10.1016/j.tws.2025.113504
Vella, D., Ajdari, A., Vaziri, A., Boudaoud, A., 2011. Wrinkling of pressurized elastic shells. Phys. Rev. Lett. 107, 174301. https://doi.org/10.1103/PhysRevLett.107.174301
Venkata, S.P., Balbi, V., Destrade, M., Accoto, D., Zurlo, G., 2023. Programmable wrinkling for functionally-graded auxetic circular membranes. Extreme Mech. Lett. 63, 102045. https://doi.org/10.1016/j.eml.2023.102045
Venkata, S.P., Fu, Y., Fu, Y., Danesh, H., Destrade, M., Balbi, V., 2025. Wrinkling instability of 3d auxetic bilayers in tension. J. Mech. Phys. Solids , 106301. https://doi.org/10.1016/j.jmps.2025.106301
Vonach, W.K., Rammerstorfer, F.G., 2000. The effects of in-plane core stiffness on the wrinkling behavior of thick sandwiches. Acta Mech. 141 (1), 1–10. https://doi.org/10.1007/BF01176803
Wang, C., Wang, C., Huang, Z., Xu, S., 2018. Materials and structures toward soft electronics. Adv. Mater. 30 (50), 1801368. https://doi.org/10.1002/adma.201801368
Wang, G., Liu, Y., Fu, Y., 2023. A refined model for the buckling of film/substrate bilayers. Math. Mech. Solids 28 (1), 313–330. https://doi.org/10.1177/10812865221107072
Wang, Q., Zhao, X., 2013. Phase diagrams of instabilities in compressed film-substrate systems. J. Appl. Mech. 81 (5), 051004. https://doi.org/10.1115/1.4025828
Wang, T., Yang, Y., Xu, F., 2022. Mechanics of tension-induced film wrinkling and restabilization: a review. Proc. R. Soc. A . https://doi.org/10.1098/rspa.2022.0149
Webber, J.J., Worster, M.G., 2024. Wrinkling instabilities of swelling hydrogels. Phys. Rev. E 109 (4), 044602. https://doi.org/10.1103/PhysRevE.109.044602
Willis, N.J., Didier, A.K., Sonnanburg, K.M., 2008. How to compute a puiseux expansion. https://doi.org/10.48550/arXiv.0807.4674
Wong, W. S.Y., Li, M., Nisbet, D.R., Craig, V. S.J., Wang, Z., Tricoli, A., 2016. Mimosa origami: a nanostructure-enabled directional self-organization regime of materials. Sci. Adv. 2 (6), e1600417. https://doi.org/10.1126/sciadv.1600417
Wu, B., Kong, L., Chen, W., Riccobelli, D., Destrade, M., 2026. Electro-mechanical wrinkling of soft dielectric films bonded to hyperelastic substrates. J. Mech. Phys. Solids 209, 106490. https://www.sciencedirect.com/science/article/pii/S0022509625004648. https://doi.org/https://doi.org/10.1016/j.jmps.2025.106490
Xin, M., Davidovitch, B., 2021. Stretching Hookean ribbons part II: from buckling instability to far-from-threshold wrinkle pattern. Eur. Phys. J. E 44 (7), 94. https://doi.org/10.1140/epje/s10189-021-00088-9
Youn, J., Kim, D., Kwak, H., Lee, A., Kim, D.S., 2024. Tissue-scale in vitro epithelial wrinkling and wrinkle-to-fold transition. Nat. Commun. 15 (1), 7118. https://doi.org/10.1038/s41467-024-51437-z
Yue, Q., Sangwoo, K., Pence, T.J., 1994. Plane strain buckling and wrinkling of neo-hookean laminates. Int. J. Solids Struct. 31 (8), 1149–1178. https://doi.org/10.1016/0020-7683(94)90169-4
Zhang, D., Kiendl, J., 2025. A variationally consistent membrane wrinkling model based on spectral decomposition of the strain and stress tensors. J. Mech. Phys. Solids , 106331. https://doi.org/10.1016/j.jmps.2025.106331
Zhao, R., Zhang, T., Diab, M., Gao, H., Kim, K.S., 2015. The primary bilayer ruga-phase diagram i: localizations in ruga evolution. Extreme Mech. Lett. 4, 76–82. https://doi.org/10.1016/j.eml.2015.04.006
Zheng, Y., Li, G.-Y., Cao, Y., Feng, X.-Q., 2017. Wrinkling of a stiff film resting on a fiber-filled soft substrate and its potential application as tunable metamaterials. Extreme Mech. Lett. 11, 121–127. https://doi.org/10.1016/j.eml.2016.12.002
Zhou, L., Yang, L., Liu, Y., Xu, Z., Yin, J., Ge, D., Jiang, X., 2020. Dynamic structural color from wrinkled thin films. Adv. Opt. Mater. 8 (12), 2000234. https://doi.org/10.1002/adom.202000234